Topics on Interacting Ultracold Atoms in One-dimensional Systems

相互作用的超冷原子於一維系統之有關課題

MA, Kwok Wai

馬國威

A Thesis Submitted in Partial Fulfilment
of the Requirements for the Degree of
Master of Philosophy
in
Physics

The Chinese University of Hong Kong
August 2013

Thesis/Assessment Committee

Professor WANG, Dajun (Chair)
Professor LAW, Chi Kwong (Thesis Supervisor)
Professor ZHOU, Qi (Committee Member)
Professor PU, Han (External Examiner)

Abstract

Interacting bosonic atoms in one-dimensional configurations have many novel quantum mechanical properties. In the first part of the thesis, we characterize the quantum correlation for systems with two or three interacting atoms quantitatively by the Schmidt decomposition. In the second part, we consider the system with an impurity atom. When the background is a harmonically trapped Tonks-Girardeau gas, we obtain the spatial distribution for the impurity atom by evaluating its single particle density. In addition, we apply the Bogoliubov approximation to study the self-localization for an impurity atom immersed in the background with a Bose-Einstein condensate. Lastly, the dynamics of the impurity-condensate system is also examined.

摘要

一維相互作用的玻色原子系統擁有很多獨特的量子性質。在論文的首部份，我們透過Schmidt分解，量化性地描述了兩粒或三粒相互作用的原子系統之量子關聯。於第二部份，我們考慮了含有一粒雜質原子的系統。當背景是一堆囚禁於簡諧阱的Tonks-Girardeau氣體，我們通過計算雜質原子的單粒子密度，從而得出它的位置分佈。再者，我們考慮了當一粒雜質原子浸沒於玻色—愛因斯坦凝聚態之系統。利用Bogoliubov近似，我們對雜質原子的自發性位置局限作出研究。最後，我們對該系統隨時間的演化作出討論。

Acknowledgments

I would like to express my sincere gratitude to my supervisor Prof. C. K. Law, who gave me a lot of advices and supports for the research. Although he is rigorous and strict, I understand that he just wants me to improve and cultivate the right attitude toward scientific research. I always feel ashamed for my stupid and slow response to questions.

Also, I would like to thank the students, who participated in my exercise classes. It is my pleasure to learn from them. Honestly, the special tutorials and the exercise classes are very memorable and enjoyable. Hoping I can be their tutor again.

Lastly, thank my fellows in Room 224, 313 and 316. They gave me lots of cheers when I was depressed. Thank you, God.

Contents

List of Figures

List of Tables

Chapter 1

Introduction

The quantum mechanical studies on bosonic particles can be dated back to 1900. In this year, Planck obtained the formula for describing black-body radiation by assuming the discretization of energy and introducing the idea of photons. In 1924, Bose [1] successfully derived the Planck's radiation formula by proposing a new distribution for identical particles. Initially, the distribution was applied to massless particles only, in which the number of particles is unconstrained. By generalizing the idea to massive atoms with the introduction of chemical potential, Einstein [2, 3] developed the so called Bose-Einstein statistics which applies to all particles with integer values of spins. From the statistics, Einstein predicted the existence of a new phase for matter. When bosonic atoms are cooled below the critical temperature T_C, a large fraction of the atoms will be found in the ground state. This collective behaviour is called the Bose-Einstein condensation (BEC). Although the theory was proposed long time ago, it was extremely difficult to cool atoms down to such low temperature. As a result, it took a long time for the experimental preparation and realization of ultracold systems to become possible.

Thanks to the breakthrough in cooling and trapping technologies, the experimental observation of BEC finally became possible at 1995. During the experiments, alkali atoms were cooled down to microkelvin for achieving BEC

[4, 5, 6]. Apart from the success in preparing the system, the interaction between the atoms is highly controllable. All these advances provide opportunities for physicists to study and observe different quantum mechanical properties in ultracold atoms, in both weakly and strongly interacting systems. In addition, it is now possible for experimentalists to confine the transverse motion of the atoms tightly in optical traps, so that approximated one-dimensional systems can be achieved. From the lessons on quantum hall effect [7, 8], topological insulators [9] and other novel properties appeared in low-dimensional systems, it is expected that ultracold atoms in one-dimensional systems may also have some unexpected features, which cannot be observed in three-dimensional systems. The most famous example is the Tonks-Girardeau gas [10, 11]. Owing to this, we study various one-dimensional systems of ultracold atoms in this thesis.

In Chapter 2, we briefly review the system by discussing its experimental realization and introducing its effective Hamiltonian. From the Hamiltonian, we discuss the ground state of the system in the Tonks gas limit or the weakly interacting limit. After introducing the essential preliminaries, we characterize the correlation for systems of two or three interacting atoms quantitatively in Chapter 3. In Chapter 4, we consider system with an impurity atom immersed in a background filled with a harmonically trapped Tonks gas. Particularly, we focus on the spatial distribution for the impurity atom. In Chapter 5, we study the self-localization of an impurity atom immersed in a background of homogeneous BEC. In Chapter 6, we further our understanding by studying the dynamics of the impurity-condensate system. Lastly, we conclude the thesis in Chapter 7.

Chapter 2

Review on one-dimensional ultracold atomic systems

2.1 Realization of one-dimensional systems

Due to the breakthrough of atomic waveguide technology, preparation of ultracold atoms in one and two-dimensional systems are possible [12, 13, 14, 15, 16, 17]. In most cases, alkali atoms such as ^{7}Li [16], ^{23}Na [13] and ^{87}Rb [12] have been used for experimental realization of Bose-Einstein condensates in one-dimensional systems. Apart from Bose-Einstein condensates, one-dimensional spin chains in optical lattice have been prepared recently [18].

In experiments, the atoms are trapped harmonically in both transverse and longitudinal directions. For convenience, we denote the transverse directions as y and z, whereas the longitudinal direction is denoted as x. To achieve approximated one-dimensional systems, the trapping potential is highly anisotropic, with the frequency $\omega_\perp$ of the transverse potential set to a much higher value than that of the longitudinal potential. At the same time, the atoms are cooled to a sufficiently low temperature, such that the corresponding thermal energy is lower than $\hbar\omega_\perp$. Under this condition, the atoms are forbidden to transit

to higher excited states for the transverse potential. As a result, the wave function for the N-particle system can be written as [19]:

$$\Psi\left(\boldsymbol{r}_1, \boldsymbol{r}_2, \cdots, \boldsymbol{r}_N\right) = \psi\left(x_1, x_2, \cdots, x_N\right) \prod_{i=1}^{N} \phi_{0,0}\left(\boldsymbol{r}_{i\perp}\right), \tag{2.1}$$

where $\boldsymbol{r}_{i\perp} = (r_{iy}, r_{iz})$.

Since the motion in y and z is frozen by the tightly confined potential, we can just focus on the motion along x. Therefore, the system can be approximated as one-dimensional. In the following section, the effective Hamiltonian for the system will be discussed. Specifically, we try to model the effective interaction between the atoms and obtain an effective Hamiltonian for $\psi\left(x_1, x_2, \cdots, x_N\right)$.

2.2 Effective Hamiltonian for one-dimensional systems

For a system of interacting bosonic atoms with atomic mass m trapped by an external potential $V_{\text{ext}}\left(\boldsymbol{r}\right)$, the Hamiltonian is given by

$$\begin{aligned}\hat{H} = &\int \hat{\Psi}^{\dagger}\left(\boldsymbol{r}\right)\left[-\frac{\hbar^2}{2m}\nabla^2 + V_{\text{ext}}\left(\boldsymbol{r}\right)\right]\hat{\Psi}\left(\boldsymbol{r}\right)\mathrm{d}\boldsymbol{r} \\ &+ \frac{1}{2}\int \hat{\Psi}^{\dagger}\left(\boldsymbol{r}\right)\hat{\Psi}^{\dagger}\left(\boldsymbol{r'}\right)V_{\text{int}}\left(\boldsymbol{r}-\boldsymbol{r'}\right)\hat{\Psi}\left(\boldsymbol{r'}\right)\hat{\Psi}\left(\boldsymbol{r}\right)\mathrm{d}\boldsymbol{r}\mathrm{d}\boldsymbol{r'},\end{aligned} \tag{2.2}$$

where $\hat{\Psi}\left(\boldsymbol{r}\right)$ is the bosonic field operator, which annihilates an atom at the position $\boldsymbol{r}$. Here, we assume that the atoms interact with each other through the two-body interaction $V_{\text{int}}\left(\boldsymbol{r}-\boldsymbol{r'}\right)$. It is a good approximation when $r_0 \ll \rho^{-1/3}$, where r_0 is the range of the interatomic interaction and $\rho = N/V$ is the number density of the system. Under this condition, the system is said to be dilute and the three-body collision can be safely neglected. Also, it is assumed that the interaction depends on the separation between the atoms only.

When the system is dilute and the energy is low, the wave function for the relative motion between any two atoms can be approximated by the asymptotic behaviour. As a result, the actual detail of the interaction is unimportant. In this case, the scattering process between the atoms is dominated by the s-wave scattering, so the interaction can be characterized by choosing an appropriate s-wave scattering length. Due to this, the two-body interaction between the atoms is modelled by the Huang's pseudopotential [20]:

$$V_{\text{int}} = \frac{4\pi\hbar^2 a}{m}\delta^3(\boldsymbol{r})\frac{\partial}{\partial r}(r\cdot), \tag{2.3}$$

where r and a are the separation and the s-wave scattering length between the atoms respectively. The idea of the pseudopotential is summarized in Fig. 2.1.

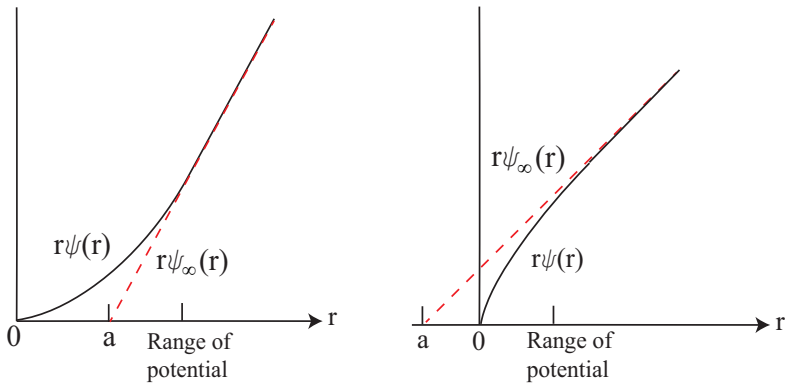

Figure 2.1: The pseudopotential for the original interaction when the s-wave scattering length is positive (left) or negative (right).

Following the common practice in experiments, we assume that the atoms are harmonically trapped in transverse directions:

$$V_{\text{trap}}^{\perp}(y,z) = \frac{1}{2}m\omega_{\perp}^2\left(y^2+z^2\right), \tag{2.4}$$

with $\omega_{\perp}$ being the angular frequency for the potential. Under this potential, the energy required to excite an atom from the ground state to the first excited state of $V_{\text{trap}}^{\perp}$ is $\hbar\omega_{\perp}$. To simplify the discussion, we first assume that the

atoms move freely in the x direction. Using the pseudopotential in (2.3), the Hamiltonian describing the scattering between two atoms is given by

$$H=\sum_{i=1}^{2}\left[-\frac{\hbar^2}{2m_i}\nabla_i^2+\frac{1}{2}m_i\omega_\perp^2\left(y_i^2+z_i^2\right)\right]+\frac{4\pi\hbar^2 a}{m}\delta^3\left(\boldsymbol{r}\right)\frac{\partial}{\partial r}\left(r\cdot\right). \tag{2.5}$$

Since the potential is harmonic, it is possible to separate the Hamiltonian into two parts as $H=H_{\mathrm{CM}}+H_{\mathrm{rel}}$, which correspond to the motion of the center of mass and the relative motion of the atoms respectively. The center of mass co-ordinates $\boldsymbol{R}$ and the relative co-ordinates $\boldsymbol{r}$ are defined as

$$\boldsymbol{R}=\frac{m_1\boldsymbol{r}_1+m_2\boldsymbol{r}_2}{m_1+m_2},\quad \boldsymbol{r}=\boldsymbol{r}_1-\boldsymbol{r}_2. \tag{2.6}$$

Using (2.6), we obtain

$$\begin{aligned}H_{\mathrm{CM}}&=-\frac{\hbar^2}{2M}\nabla_R^2+\frac{M}{2}\omega_\perp^2\left(R_y^2+R_z^2\right),\\ H_{\mathrm{rel}}&=-\frac{\hbar^2}{2\mu}\nabla_r^2+\frac{\mu}{2}\omega_\perp^2\left(r_y^2+r_z^2\right)+\frac{4\pi\hbar^2 a}{m}\delta^3\left(\boldsymbol{r}\right)\frac{\partial}{\partial r}\left(r\cdot\right),\end{aligned} \tag{2.7}$$

with $M=m_1+m_2$ and $\mu=m_1m_2/\left(m_1+m_2\right)$ being the total mass and the reduced mass for the two atoms respectively.

Focusing on the relative motion, we consider an incident atom with wave function $\psi_{\mathrm{inc}}\left(\boldsymbol{r}\right)=e^{ik_{r_x}r_x}\phi_{0,0}\left(r_y,r_z\right)$, which is the single-particle ground state of H_{rel}. As mentioned in Section 2.1, the transverse motion is frozen by lowering the temperature of the system. More precisely, the kinetic energy along the x direction satisfies

$$\frac{\hbar^2k_{r_x}^2}{2\mu}<2\hbar\omega_\perp. \tag{2.8}$$

Using the partial wave expansion, the scattered wave function at $x\to\infty$ is given by [21]

$$\psi_{\mathrm{sc}}\left(\boldsymbol{r}\right)=\left[e^{ik_{r_x}r_x}+f_{\mathrm{even}}e^{ik_{r_x}|r_x|}+f_{\mathrm{odd}}\mathrm{sign}\left(r_x\right)e^{ik_{r_x}|r_x|}\right]\phi_{0,0}\left(r_y,r_z\right), \tag{2.9}$$

where f_{even} and f_{odd} are the one-dimensional scattering amplitudes for the even and the odd partial waves respectively. When the condition in (2.8) is

satisfied, it is reminded that $\phi(r_y, r_z)$ cannot be transmitted to higher excited state. In this case, the effective one-dimensional scattering length was found to be [21]

$$a_{1D} = -\frac{a_\perp^2}{2a}\left(1 - \mathcal{C}\frac{a}{a_\perp}\right), \tag{2.10}$$

where $a_\perp = \sqrt{\hbar/(\mu\omega_\perp)}$ and $\mathcal{C} = |\zeta(1/2)|/\sqrt{2} \approx 1.4603$. In the low velocity regime $k_{r_x} a_\perp \ll 1$, the scattering amplitudes are approximated as

$$f_{\text{odd}} = 0, \quad f_{\text{even}} = -\frac{1}{1 + ik_{r_x} a_{1D}}, \tag{2.11}$$

which suggests that the effective interaction between the atoms can be modelled as

$$U(r_x) = g\delta(r_x). \tag{2.12}$$

More importantly, the effective coupling strength is given by

$$g = -\frac{\hbar^2}{\mu a_{1D}} = \frac{2\hbar^2 a}{\mu a_\perp^2}\frac{1}{(1 - \mathcal{C}a/a_\perp)}. \tag{2.13}$$

To summarize, the interaction between the atoms for the approximated one-dimensional system can be modelled by the Dirac delta potential, which is a generalization of the Lieb-Liniger model [22, 23]. Using (2.12), the effective Hamiltonian describing an one-dimensional system with N ultracold atoms is

$$H = \sum_{i=1}^{N}\left[-\frac{\hbar^2}{2m}\frac{\partial^2}{\partial x_i^2} + V_{\text{ext}}(x_i)\right] + \sum_{i<j}^{N} g\delta(x_i - x_j), \tag{2.14}$$

where V_{ext} is the external potential along the x direction. From (2.14), it is observed that the interaction between the atoms is characterized by the single parameter g defined in (2.13) only. It is possible to control the interaction between the atoms by tuning the scattering length a through magnetic or optical Feshbach resonance [24, 25, 26, 27]. Apart from tuning the scattering length, it is possible to control the interaction by altering the trapping frequency of the transverse potential also. Therefore, the tunability of the system is extremely high, which provides opportunities for physicists to investigate different physical properties in both strongly interacting and weakly interacting regimes.

2.3 Ground state: Tonks gas systems

For ultracold bosonic atoms in one-dimensional systems, the Tonks gas limit ($g \to \infty$) has attracted lots of attention [28, 29, 30, 31, 32, 33]. In this limit, the atoms are infinitely repulsive and the corresponding system is named as Tonks-Girardeau gas or Tonks gas in short. Since the motion of the atoms is confined in one dimension, the atoms cannot occupy the same position, so that the energy of the system can be minimized. Therefore, the atoms are impenetrable and the system mimics the system of non-interacting spinless fermions. Particularly, if all the atoms have the same atomic mass m and trapped by the same potential $V(x_i)$, then the time-independent Schrödinger's equation for the system is given by

$$\sum_{i=1}^{N}\left[-\frac{\hbar^2}{2m}\frac{\partial^2}{\partial x_i^2}+V(x_i)\right]\Psi(x_1,x_2,\cdots,x_N)=E\Psi(x_1,x_2,\cdots,x_N), \quad (2.15)$$

with the boundary condition that $\Psi(x_1,x_2,\cdots,x_N)=0$ when $x_i=x_j\,(i\neq j)$. This boundary value problem is equivalent to solve the time-independent Schrödinger's equation for N identical non-interacting spinless fermions. Guided by this, the solution to the Tonks gas system is provided by the Bose-Fermi mapping theorem [10].

Denote the ground state wave functions for the Tonks gas system and the non-interacting fermionic system as Ψ_B and Ψ_F respectively. The Bose-Fermi mapping theorem relates them as

$$\Psi_B(x_1,x_2,\cdots,x_N)=\mathcal{A}(x_1,x_2,\cdots,x_N)\,\Psi_F(x_1,x_2,\cdots,x_N). \quad (2.16)$$

Here, Ψ_F is the $N\times N$ Slater determinant for the fermionic system:

$$\Psi_F(x_1,x_2,\cdots,x_N)=\frac{1}{\sqrt{N!}}\begin{vmatrix}\psi_0(x_1) & \psi_0(x_2) & \cdots & \psi_0(x_N)\\ \psi_1(x_1) & \psi_1(x_2) & \cdots & \psi_1(x_N)\\ \vdots & \vdots & \ddots & \vdots\\ \psi_N(x_1) & \psi_N(x_2) & \cdots & \psi_N(x_N)\end{vmatrix}, \quad (2.17)$$

with $\psi_n(x_i)$ being the n-th excited state for the single particle Hamiltonian:

$$h_i = -\frac{\hbar^2}{2m}\frac{\partial^2}{\partial x_i^2} + V_{\text{ext}}(x_i). \tag{2.18}$$

In addition, the antisymmetric function $\mathcal{A}$ is defined as

$$\mathcal{A}(x_1, x_2, \cdots, x_N) = \prod_{j>i} \text{sign}(x_j - x_i). \tag{2.19}$$

The idea behind the theorem is clear. First, the antisymmetric Slater determinant ensures that $\Psi_B(x_1, x_2, \cdots, x_N) = 0$ whenever $x_i = x_j$ $(i \neq j)$, and Ψ_B is a solution of (2.15). In order to symmetrize the wave function, the antisymmetric function $\mathcal{A}$ is introduced. From (2.16), it is noticed that the probability amplitudes $|\Psi_B|^2$ and $|\Psi_F|^2$ are the same. Hence, all physical quantities which depend solely on the spatial probability will be the same for both systems. Although both systems share many common features, they are not identical to each other. For examples, the quantum correlation appeared in the off-diagonal elements for the reduced single particle density matrix and the momentum distribution for the systems are different [28, 32].

2.3.1 Tonks gas in a harmonic potential

In this subsection, we summarize some important results for the ground state of the harmonically trapped Tonks gas system. First, the wave function of the system can be simplified into [30]

$$\Psi(x_1, x_2, \cdots, x_N) = \mathcal{N}\prod_{i=1}^{N} e^{-x_i^2/2} \prod_{1\leq j<k\leq N} |x_k - x_j|, \tag{2.20}$$

with x_i in the unit of $x_{osc} = \sqrt{\hbar/(m\omega)}$. The normalization constant $\mathcal{N}$ is given explicitly by

$$\mathcal{N} = 2^{\frac{N(N-1)}{4}} N! \left[\prod_{n=0}^{N-1} n!\sqrt{\pi}\right]^{-1/2}. \tag{2.21}$$

The single particle density, which is proportional to the probability of finding an atom in x, is defined as

$$\rho(x) = N \int |\Psi(x_1, x_2, \cdots, x_N)|^2 \, \mathrm{d}x_2 \mathrm{d}x_3 \cdots \mathrm{d}x_N. \tag{2.22}$$

The explicit result for the system of Tonks gas is [30]

$$\rho(x) = \sum_{n=1}^{N-1} |\psi_n(x)|^2 . \tag{2.23}$$

The pair distribution function, which is proportional to the joint probability of finding an atom in x_1 and another atom in x_2, is defined as

$$D(x_1, x_2) = N(N-1) \int |\Psi(x_1, x_2, \cdots, x_N)|^2 \, \mathrm{d}x_3 \mathrm{d}x_4 \cdots \mathrm{d}x_N. \tag{2.24}$$

For the present system, we have [30]

$$D(x_1, x_2) = \sum_{0 \le n < n' \le N-1} |\psi_n(x_1)\psi_{n'}(x_2) - \psi_n(x_2)\psi_{n'}(x_1)| . \tag{2.25}$$

It is reminded that both the single particle density and the pair distribution function can be applied to the Tonks gas system and the non-interacting fermionic system.

Lastly, we want to remark that Tonks gas is not just an idealized theoretical model. Experimental observation for the systems have been reported [34, 35]. Also, transport of spin impurity atoms in Tonks gas has also been studied experimentally [36].

2.4 Ground state: Weakly interacting systems

The effective Hamiltonian for the approximated one-dimensional systems is

$$\begin{aligned} \hat{H} = & \int \hat{\Psi}^\dagger(x) \left[-\frac{\hbar^2}{2m} \frac{\partial^2}{\partial x^2} + V(x) \right] \hat{\Psi}(x) \, \mathrm{d}x \\ & + \frac{1}{2} \int \hat{\Psi}^\dagger(x) \hat{\Psi}^\dagger(x') U(x - x') \hat{\Psi}(x') \hat{\Psi}(x) \, \mathrm{d}x \mathrm{d}x', \end{aligned} \tag{2.26}$$

where $V(x)$ and $U(x-x')$ stand for the trapping potential and the two-body interaction between the atoms respectively. In later studies, the interaction between the atoms will be modelled by the effective Dirac delta potential $g\delta(x_j - x_i)$, which has been discussed in Section 2.2. Then, the Hamiltonian is simplified into

$$\hat{H} = \int \hat{\Psi}^\dagger(x) \left[-\frac{\hbar^2}{2m}\frac{\partial^2}{\partial x^2} + V(x) \right] \hat{\Psi}(x)\,\mathrm{d}x + \frac{g}{2}\int \hat{\Psi}^\dagger(x)\,\hat{\Psi}^\dagger(x)\,\hat{\Psi}(x)\,\hat{\Psi}(x)\,\mathrm{d}x. \tag{2.27}$$

2.4.1 Mean field solution

When the temperature of the system is sufficiently low, a large fraction of the atoms will be found in the ground state. As the first approximation, we neglect the fluctuations and replace the field operator by the macroscopic wave function $\Psi(x)$ [37]. This procedure is called the mean field approach, in which the Hamiltonian in (2.27) reduces to

$$H = \int \Psi^*(x) \left[-\frac{\hbar^2}{2m}\frac{\partial^2}{\partial x^2} + V(x) \right] \Psi(x)\,\mathrm{d}x + \frac{g}{2}\int \Psi^*(x)\,\Psi^*(x)\,\Psi(x)\,\Psi(x)\,\mathrm{d}x. \tag{2.28}$$

The mean field solution is determined by minimizing H with respect to $\Psi(x)$ and $\Psi^*(x)$, which gives the time independent Gross-Pitaevskii equation:

$$\left[-\frac{\hbar^2}{2m}\frac{\partial^2}{\partial x^2} + V(x) + g\left|\Psi(x)\right|^2 - \mu \right] \Psi(x) = 0. \tag{2.29}$$

Here, the chemical potential μ is introduced to conserve the number of atoms.

2.4.2 Bogoliubov theory: Trapping condensates

To go beyond the mean field solution, we separate the field operator into the mean field solution and the fluctuation operator as

$$\hat{\Psi}(x) = \Psi(x) + \delta\hat{\Psi}(x), \tag{2.30}$$

In the Bogoliubov theory, the Hamiltonian is linearized by keeping terms up to second order in the fluctuation. The Hamiltonian with zeroth order in the fluctuation is the mean field Hamiltonian in (2.28). The Hamiltonian with first order in the fluctuation vanishes as $\Psi(x)$ satisfies (2.29). The Hamiltonian with second order in fluctuation is

$$\begin{aligned}\hat{H} = &\int \delta\hat{\Psi}^{\dagger}(x)\left[-\frac{\hbar^2}{2m}\frac{\partial^2}{\partial x^2}+V(x)\right]\delta\hat{\Psi}(x)\,\mathrm{d}x \\ &+\frac{g}{2}\int|\Psi(x)|^2\left[\delta\hat{\Psi}(x)\,\delta\hat{\Psi}(x)+4\delta\hat{\Psi}^{\dagger}(x)\,\delta\hat{\Psi}(x)+\delta\hat{\Psi}^{\dagger}(x)\,\delta\hat{\Psi}^{\dagger}(x)\right]\mathrm{d}x.\end{aligned} \tag{2.31}$$

Focusing on the time-independent case, the linearized equations for the field operators are given by

$$\begin{aligned}&\left[-\frac{\hbar^2}{2m}\frac{\partial^2}{\partial x^2}+V(x)+2g|\Psi(x)|^2-\mu\right]\delta\hat{\Psi}(x)+g|\Psi(x)|^2\delta\hat{\Psi}^{\dagger}(x)=0,\\ &\left[-\frac{\hbar^2}{2m}\frac{\partial^2}{\partial x^2}+V(x)+2g|\Psi(x)|^2-\mu\right]\delta\hat{\Psi}^{\dagger}(x)+g|\Psi(x)|^2\delta\hat{\Psi}(x)=0.\end{aligned} \tag{2.32}$$

To solve the coupled equations, we carry out the Bogoliubov transformation

$$\delta\hat{\Psi}(x)=\sum_i\left[u_i(x)\,\hat{c}_i-v_i^*(x)\,\hat{c}_i^{\dagger}\right], \tag{2.33}$$

with $\hat{c}_i$ and $\hat{c}_i^{\dagger}$ being the bosonic operators which creates and destroys an excitation in the states i respectively. In addition, they satisfy the commutation relation:

$$\left[\hat{c}_i,\hat{c}_i^{\dagger}\right]=1. \tag{2.34}$$

Substituting (2.33) into (2.32), we obtain the Bogoliubov-de Gennes (BdG) equations for $u_i(x)$ and $v_i(x)$:

$$\begin{aligned}&\left[-\frac{\hbar^2}{2m}\frac{\partial^2}{\partial x^2}+V(x)+2g|\Psi(x)|^2-\mu\right]u_i(x)-g|\Psi(x)|^2v_i(x)=0,\\ &\left[-\frac{\hbar^2}{2m}\frac{\partial^2}{\partial x^2}+V(x)+2g|\Psi(x)|^2-\mu\right]v_i(x)-g|\Psi(x)|^2u_i(x)=0.\end{aligned} \tag{2.35}$$

Here, $u_i(x)$ and $v_i(x)$ satisfy the orthogonality condition:

$$\int \left[u_i(x)\, u_j^*(x) - v_i(x)\, v_j^*(x)\right] \mathrm{d}x = 0, \tag{2.36}$$

and the normalization condition

$$\int \left[|u_i(x)|^2 - |v_i(x)|^2\right] = 1. \tag{2.37}$$

Using the solution for (2.35), the Hamiltonian in (2.31) can be diagonalized as

$$\hat{H} = E_0 + \sum_i \epsilon_i \hat{c}_i^\dagger \hat{c}_i. \tag{2.38}$$

Finally, the ground state of the system at zero temperature corresponds to the vacuum state:

$$\hat{c}_i |0\rangle = 0, \quad \forall i. \tag{2.39}$$

2.4.3 Homogeneous condensates

In chapter 5 and 6, the trapping potential for the condensate is assumed to be very weak $V(x) \approx 0$, so that the condensate is approximated to be homogeneous. Different from the trapping system, we go beyond the mean field solution by expanding the field operator using the plane wave basis directly:

$$\hat{\Psi}(x) = \sum_k \hat{a}_k \frac{e^{ikx}}{\sqrt{l}}, \tag{2.40}$$

where l is the length of the one-dimensional system. Then, the Hamiltonian becomes:

$$\hat{H} = \sum_k \frac{\hbar^2 k^2}{2m} \hat{a}_k^\dagger \hat{a}_k + \frac{g}{2l} \sum_{k_1,k_2,q} \hat{a}_{k_1+q}^\dagger \hat{a}_{k_2-q}^\dagger \hat{a}_{k_1} \hat{a}_{k_2}, \tag{2.41}$$

where $\hat{a}_k^\dagger$ stands for the bosonic creation operator, which creates a particle in the state with momentum $p = \hbar k$. The commutation relation is

$$\left[\hat{a}_k, \hat{a}_{k'}^\dagger\right] = \delta_{k,k'}. \tag{2.42}$$

In the Bogoliubov approximation, we first separate $\hat{a}_0$ for the ground state out and retain terms up to second order in $\hat{a}_k$ with $k \neq 0$, so the Hamiltonian becomes

$$\begin{aligned}\hat{H} = &\sum_{k\neq 0} \frac{\hbar^2 k^2}{2m} \hat{a}_k^\dagger \hat{a}_k + \frac{g}{2l} \hat{a}_0^\dagger \hat{a}_0^\dagger \hat{a}_0 \hat{a}_0 \\ &+ \frac{g}{2l} \sum_{k\neq 0} \left(\hat{a}_0 \hat{a}_0 \hat{a}_k^\dagger \hat{a}_{-k}^\dagger + 4 \hat{a}_0^\dagger \hat{a}_k^\dagger \hat{a}_0 \hat{a}_k + \hat{a}_0^\dagger \hat{a}_0^\dagger \hat{a}_k \hat{a}_{-k} \right). \end{aligned} \tag{2.43}$$

Then, we replace $\hat{a}_0 = \hat{a}_0^\dagger = \sqrt{N}$. However, we need to be careful of the normalization condition:

$$\hat{a}_0^\dagger \hat{a}_0 + \sum_{k\neq 0} \hat{a}_k^\dagger \hat{a}_k = N, \tag{2.44}$$

which leads to

$$\hat{a}_0^\dagger \hat{a}_0^\dagger \hat{a}_0 \hat{a}_0 = N^2 - 2N \sum_{k\neq 0} a_k^\dagger a_k. \tag{2.45}$$

The Bogoliubov approximated Hamiltonian becomes:

$$\hat{H} = \frac{gnN}{2} + \sum_{k\neq 0} \frac{\hbar^2 k^2}{2m} \hat{a}_k^\dagger \hat{a}_k + \frac{gn}{2} \sum_{k\neq 0} \left(2\hat{a}_k^\dagger \hat{a}_k + \hat{a}_k^\dagger \hat{a}_{-k}^\dagger + \hat{a}_k \hat{a}_{-k} \right), \tag{2.46}$$

where $n = N/l$ is the number density of the atoms.

The Hamiltonian in (2.46) can be diagonalized by the Bogoliubov transformation:

$$\begin{aligned} \hat{a}_k &= u_k \hat{c}_k - v_k \hat{c}_{-k}^\dagger, \\ \hat{a}_{-k} &= u_k \hat{c}_{-k} - v_k \hat{c}_k^\dagger. \end{aligned} \tag{2.47}$$

In order to satisfy the commutation relation in (2.42), u_k and v_k must satisfy

$$u_k^2 - v_k^2 = 1. \tag{2.48}$$

Here, we have assumed u_k and v_k are real. After the Bogoliubov transformation, the Hamiltonian becomes

$$\begin{aligned}\hat{H} =&\frac{gnN}{2}+\sum_{k\neq 0}\left[\frac{\hbar^2k^2}{2m}v_k^2+gn\left(v_k^2-u_kv_k\right)\right]\\&+\sum_{k\neq 0}\left[\left(\frac{\hbar^2k^2}{2m}+gn\right)\left(u_k^2+v_k^2\right)-2gnu_kv_k\right]\hat{c}_k^\dagger c_k\\&+\sum_{k\neq 0}\left[\frac{gn}{2}\left(u_k^2-2u_kv_k+v_k^2\right)-\frac{\hbar^2k^2}{2m}u_kv_k\right]\left(\hat{c}_k^\dagger\hat{c}_{-k}^\dagger+\hat{c}_k\hat{c}_{-k}\right).\end{aligned}\tag{2.49}$$

To eliminate the last term, we can choose

$$\frac{gn}{2}\left(u_k^2-2u_kv_k+v_k^2\right)-\frac{\hbar^2k^2}{2m}u_kv_k=0.\tag{2.50}$$

On solving (2.48) and (2.50), we obtain

$$u_k=\sqrt{\frac{1}{2}\left[\frac{gn+\epsilon\left(k\right)}{\xi\left(k\right)}+1\right]}\quad\text{and}\quad v_k=\sqrt{\frac{1}{2}\left[\frac{gn+\epsilon\left(k\right)}{\xi\left(k\right)}-1\right]},\tag{2.51}$$

where $\epsilon\left(k\right)=\hbar k^2/\left(2m\right)$ and $\xi\left(k\right)=\sqrt{\epsilon\left(k\right)\left[\epsilon\left(k\right)+2gn\right]}$ are the dispersion relations for free particles and Bogoliubov excitations respectively. Finally, we obtain the Bogoliubov Hamiltonian for the ground state of the weakly interacting system:

$$\hat{H}=E_0+\sum_{k\neq 0}\xi\left(k\right)\hat{c}_k^\dagger\hat{c}_k.\tag{2.52}$$

Here, $\hat{c}_k^\dagger$ is the quasi-particle operator, which creates a Bogoliubov excitation with wavenumber k. Physically, (2.52) shows that the system of interacting atoms can be described by a collection of independent quasi-particles, in which the energy obeys the Bogoliubov spectrum $\xi\left(k\right)$. Finally, the ground state of the system at zero temperature corresponds to the vacuum state of the quasi-particles:

$$\hat{c}_k\left|0\right\rangle=0,\quad\forall k\neq 0.\tag{2.53}$$

Chapter 3

Correlation for two or three interacting atoms in 1D systems

Nowadays, extraction of few atoms in optical traps is feasible [38, 39], which provides opportunities on studying quantum mechanical properties for few-atom systems. In this chapter, we focus on the correlation for systems of two or three interacting atoms [40, 41, 42, 43, 44] by applying the effective Hamiltonian for one-dimensional systems in (2.14). To characterize the correlation quantitatively, we perform Schmidt decomposition for the ground state wave function. Using the result, the purities and the entropies for the system at different values of g are evaluated. In order to address the correlation due to the interaction, the second order coherence function for the system is introduced. Following the above procedures, we can understand how the correlation in the system changes as the coupling constant transits from $g = 0$ to $g \to \infty$.

3.1 Two-atom system

First, we consider the system of two harmonically trapped interacting atoms. The atoms are identical and each of them has atomic mass m. The

effective Hamiltonian is given by [44]

$$H = -\frac{\hbar^2}{2m}\left(\frac{\partial^2}{\partial x_1^2} + \frac{\partial^2}{\partial x_2^2}\right) + \frac{1}{2}m\omega^2\left(x_1^2 + x_2^2\right) + g\delta\left(x_2 - x_1\right). \tag{3.1}$$

For simplification, the length is rescaled as $\tilde{x} = x/\sqrt{\hbar/\left(m\omega\right)}$. Then, the rescaled Hamiltonian is dimensionless and it is given by

$$\tilde{H} = -\frac{1}{2}\left(\frac{\partial^2}{\partial \tilde{x}_1^2} + \frac{\partial^2}{\partial \tilde{x}_2^2}\right) + \frac{1}{2}\left(\tilde{x}_1^2 + \tilde{x}_2^2\right) + \tilde{g}\delta\left(\tilde{x}_2 - \tilde{x}_1\right). \tag{3.2}$$

Here, the energy is measured in unit of $\hbar\omega$ and the rescaled coupling strength is given by $\tilde{g} = g\sqrt{m/\left(\hbar^3\omega\right)}$. Without ambiguity, the rescaled units will be used for the remaining discussion and the tildes over them will be dropped.

3.1.1 Analytic solution to the Hamiltonian

By defining the new variables:

$$R = \frac{1}{\sqrt{2}}\left(x_1 + x_2\right), \quad r = \frac{1}{\sqrt{2}}\left(x_2 - x_1\right), \tag{3.3}$$

then the Hamiltonian in (3.2) can be separated into $H = H_{\mathrm{CM}} + H_{\mathrm{rel}}$, which are defined as

$$\begin{aligned} H_{\mathrm{CM}} &= -\frac{1}{2}\frac{\partial^2}{\partial R^2} + \frac{1}{2}R^2, \\ H_{\mathrm{rel}} &= -\frac{1}{2}\frac{\partial^2}{\partial r^2} + \frac{1}{2}r^2 + \frac{g}{\sqrt{2}}\delta\left(r\right). \end{aligned} \tag{3.4}$$

Clearly, the solutions to the equation $H_{\mathrm{CM}}\phi\left(R\right) = E_R\phi\left(R\right)$ are given by the solutions to the harmonic oscillator problem. For $H_{\mathrm{rel}}\psi\left(r\right) = E_r\psi\left(r\right)$, there are two possible types of solutions. For the antisymmetric solutions (odd excited states), the energies and the wave functions are the same as the ordinary harmonic oscillator. It is because the antisymmetric wave functions must vanish at $x_1 = x_2$, which eliminates the coupling between the atoms. However, this kind of solutions are forbidden as the wave function must be symmetric under the exchange in x_1 and x_2. For the symmetric solutions, the case is much

complicated. The eigenenergies are governed by the transcendental equation [45]:

$$\frac{\Gamma\left(-\frac{E_r}{2}+\frac{3}{4}\right)}{\Gamma\left(-\frac{E_r}{2}+\frac{1}{4}\right)}=-\frac{g}{2\sqrt{2}}, \tag{3.5}$$

and the corresponding eigenfunctions are

$$\psi(r)=\mathcal{N}e^{-r^2/2}U\left(\frac{1}{4}-\frac{E_r}{2},\frac{1}{2},r^2\right). \tag{3.6}$$

Here, $\mathcal{N}$ is the normalization factor and $U(\mu,\nu,r^2)$ is the Kummer's confluent hypergeometric function [46]. The energy spectrum for the system $E=E_R+E_r$ against the coupling strength g is plotted in Fig. 3.1. Apart from the energy spectrum, the ground state wave functions for the system at various values of g are plotted in Fig. 3.2. It is clear that the wave functions vanish at $x_1=x_2$ gradually as g increases from 0 to the Tonks gas limit.

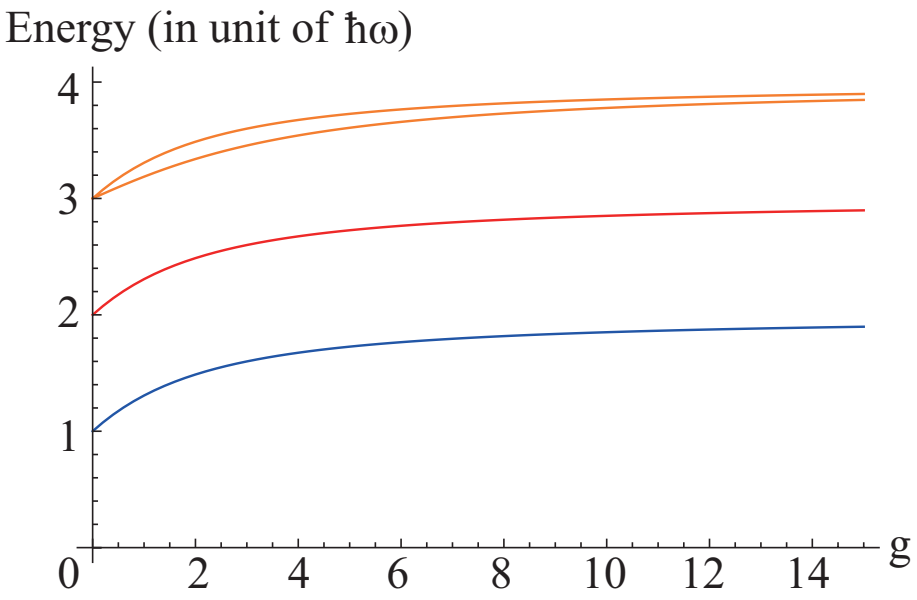

Figure 3.1: Energy spectrum for the two-atom system against g.

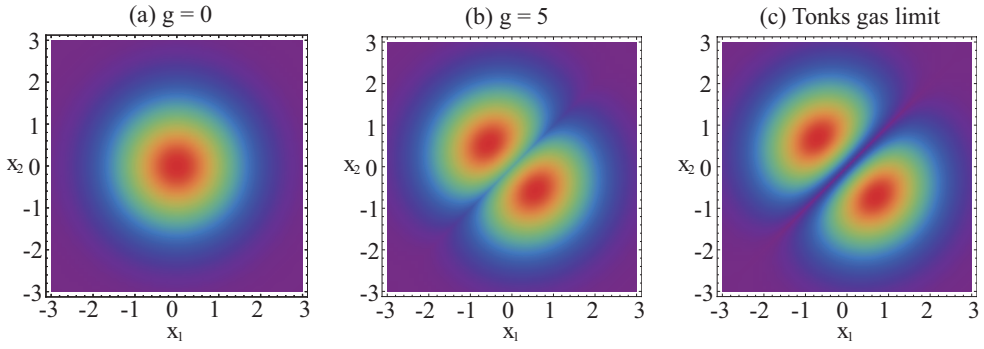

Figure 3.2: The ground state wave functions for the two-atom system.

3.1.2 Schmidt decomposition

After finding the ground state wave function, we consider the RSPDM for the system. It is defined as

$$\rho_1(x, x') = \langle \hat{\Psi}^\dagger(x)\, \hat{\Psi}(x') \rangle, \tag{3.7}$$

which specifies the correlation between the two points x and x'. To write the definition in terms of the wave function, we have

$$\rho_1(x, x') = N \int \Psi^*(x, x_2, \cdots, x_N)\, \Psi(x', x_2, \cdots, x_N)\, \mathrm{d}x_2 \mathrm{d}x_3 \cdots \mathrm{d}x_N. \tag{3.8}$$

Here, the normalization condition is $\int \rho_1(x, x) = N$. We have plotted several RSPDMs in Fig. 3.3. Clearly, the system has no correlation when $g = 0$, which is illustrated by the isotropy of the RSPDM. As g increases, the isotropy fades out and the peak squeezes along the diagonal direction gradually. Also, the peak starts to separate and two separate peaks are formed. These observations illustrate the correlation for the system.

To study the correlation more quantitatively, we consider the Schmidt decomposition of the wave function. The Schmidt decomposition for the two-atom system is defined as [47]

$$\Psi(x_1, x_2) = \sum_i \sqrt{\lambda_i} u_i(x_1)\, u_i(x_2). \tag{3.9}$$

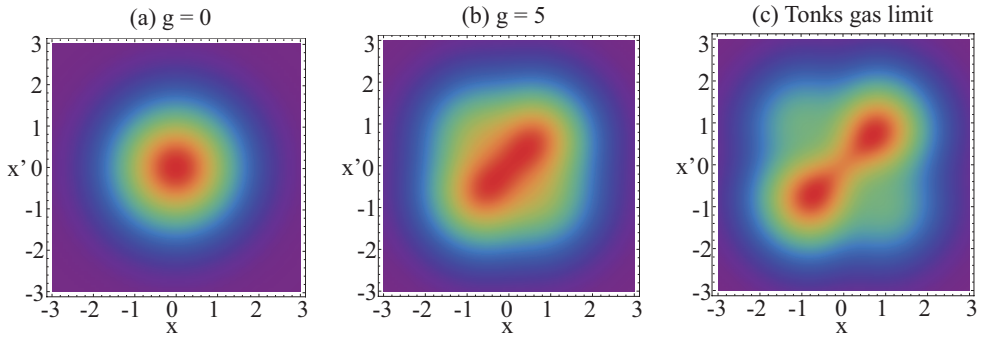

Figure 3.3: RSPDMs for the ground state of the two-atom system.

Using the RSPDM, the Schmidt coefficients λ_i and the Schmidt modes $u_i(x_i)$ are defined as

$$\int_{-\infty}^{\infty} \rho_1(x, x')\, u_i(x')\, \mathrm{d}x' = \lambda_i u_i(x)\,. \tag{3.10}$$

In practice, the RSPDM is discretized, so that the continuous equation is turned into an eigenvalue problem for a finite matrix. If the atoms are uncorrelated, the ground state wave function can be factorized, so only one term for λ_i survives. If the RSPDM is normalized to 1, the non-vanishing term is exactly 1. On the other hand, the wave function cannot be factorized if the atoms are correlated. Hence, more than one Schmidt coefficients are non-zero. For illustration, we plot the largest four Schmidt coefficients and their sum against the coupling strength in Fig. 3.4.

First, we see that the fourth largest Schmidt coefficients are nearly zero when $g = 0$ to $g = 15$. Also, the sum is nearly one for $g = 0$ to $g = 15$. Indeed, it drops slowly against g, which is difficult to visualize. Specifically, the sum is about 0.996 when $g = 15$. These observations suggest that about three Schmidt modes are necessary to describe the ground state of the system. In addition, the most occupied Schmidt modes for various values of g are plotted in Fig. 3.5.

To go one step further, we define the purity for the system as

$$\mathcal{P} = \mathrm{Tr}\left(\rho_1^2\right) \tag{3.11}$$

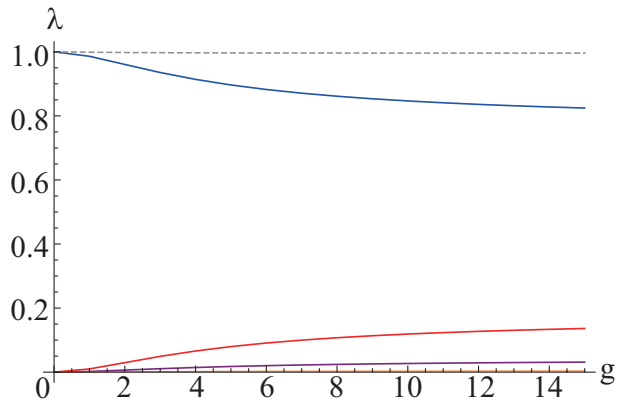

Figure 3.4: Largest four Schmidt coefficients (solid lines) and their sum (dashed line) for the ground state of the two-atom system.

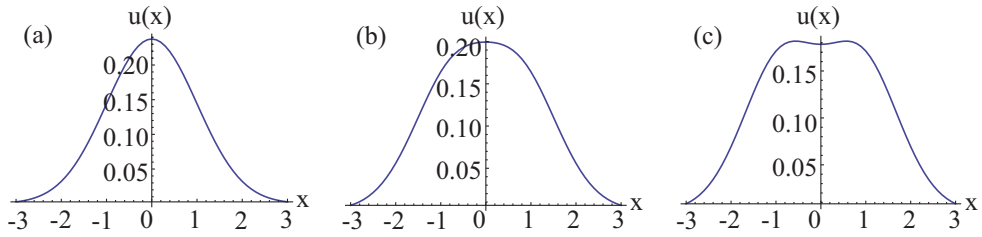

Figure 3.5: The most occupied Schmidt modes $u(x)$ for the ground state of the two-atom system when (a) $g = 0$, (b) $g = 5$ and (c) $g \to \infty$.

and the entropy as

$$S = -\sum_i \lambda_i \ln \lambda_i. \tag{3.12}$$

Clearly, $\mathcal{P} = 1$ and $S = 0$ for an uncorrelated system. Also, S is larger if more Schmidt modes are necessary to describe the wave function for the system. Therefore, we can quantify the correlation for the system by evaluating S. The purity and the entropy for the system against the coupling strength are plotted in Fig. 3.6.

Although S is named entropy of entanglement for bipartite systems of distinguishable particles, special care is needed for systems of identical particles.

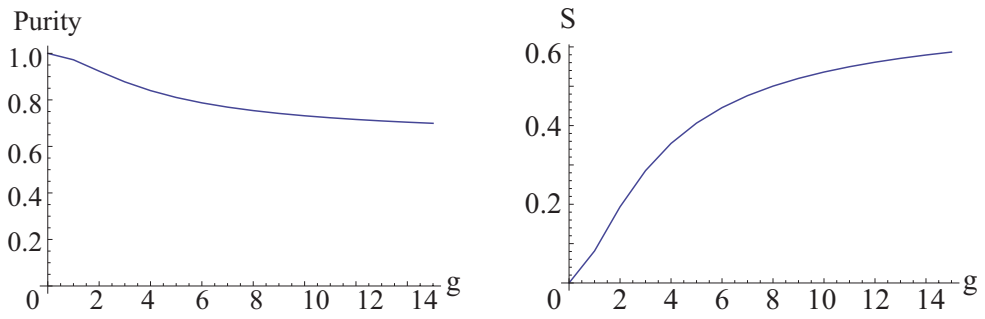

Figure 3.6: Purity (left) and the entropy (right) for the ground state of the two-atom system against g.

It is because the symmetrization postulate directly introduces an intrinsic non-separability to the wave functions [48]. The idea of detector-level entanglement for identical particles has been introduced recently [49]. However, the issue is not completely solved and it is still an open problem.

3.1.3 Second order coherence function

Apart from $\mathcal{P}$ and S, we evaluate the second order coherence function $G^{(2)}(x_1, x_2)$, which is defined as

$$G^{(2)}(x_1, x_2) = \frac{\int |\Psi|^2 \mathrm{d}x_3 \mathrm{d}x_4 \cdots \mathrm{d}x_N}{\left(\int |\Psi|^2 \mathrm{d}x_2 \mathrm{d}x_3 \cdots \mathrm{d}x_N\right)\left(\int |\Psi|^2 \mathrm{d}x_1 \mathrm{d}x_3 \cdots \mathrm{d}x_N\right)}. \tag{3.13}$$

Here, the numerator gives the joint probability of finding two atoms at x_1 and x_2 simultaneously. The denominator is the product for the probabilities of finding one atom at x_1 and one atom at x_2 separately. When $g > 0$, the joint probability for finding two atoms in x_1 and x_2 simultaneously is said to be enhanced (reduced) if $G^{(2)}(x_1, x_2)$ is greater (smaller) than one.

For example, we evaluate $G^{(2)}(x_1, x_2)$ at various values of g and plot the results in Fig. 3.7. We see that coherence builds up when g increases from zero to infinity. Particularly, we obtain an analytic expression for the Tonks gas limit:

$$G^{(2)}(x_1, x_2) = \frac{4(x_1 - x_2)^2}{(1 + 2x_1^2)(1 + 2x_2^2)}. \tag{3.14}$$

From (3.14), we find that the correlation is strongest along the line $x_1 x_2 = -1/2$, with $G^{(2)}(x_1, x_2) = 2$. Therefore, the joint probability of finding the two atoms at these positions simultaneously is doubled. In contrast, the probability of finding the atoms at the same position is zero, which is an expected result for Tonks gas.

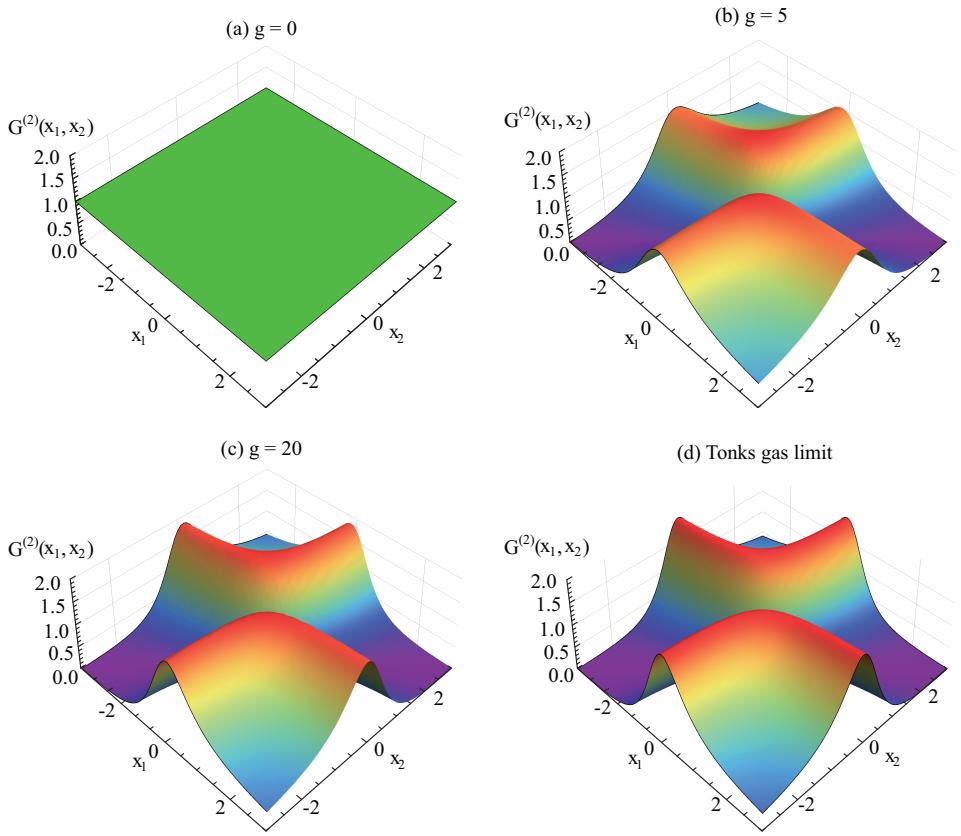

Figure 3.7: Second order coherence functions for the two-atom system.

3.2 Three-atom system

In this section, we further our studies by considering system of three harmonically trapped interacting atoms. The differences from the two-atom system is addressed.

3.2.1 Changing coordinates

The Hamiltonian for the three-atom system is given by

$$H=\sum_{i=1}^{3}\left(-\frac{1}{2}\frac{\partial^2}{\partial x_i^2}+\frac{x_i^2}{2}\right)+g\sum_{1\leq i<j\leq 3}\delta\left(x_j-x_i\right), \tag{3.15}$$

which cannot be diagonalized analytically, so an effective numerical method is necessary. Before discussing the numerical details, we introduce a new set of coordinates to simplify the problem.

First, the center of mass can be separated out from the Hamiltonian. We consider the following coordinate system:

$$\begin{pmatrix} R \\ X \\ Y \end{pmatrix}=\begin{pmatrix} \frac{1}{\sqrt{3}} & \frac{1}{\sqrt{3}} & \frac{1}{\sqrt{3}} \\ \frac{1}{\sqrt{2}} & -\frac{1}{\sqrt{2}} & 0 \\ -\frac{1}{\sqrt{6}} & -\frac{1}{\sqrt{6}} & \sqrt{\frac{2}{3}} \end{pmatrix}\begin{pmatrix} x_1 \\ x_2 \\ x_3 \end{pmatrix}. \tag{3.16}$$

In the new coordinate system, the Hamiltonian can be separated into $H = H_R + H_{X,Y}$ with H_R and $H_{X,Y}$ defined as

$$H_R=-\frac{1}{2}\frac{\partial^2}{\partial R^2}+\frac{1}{2}R^2, \tag{3.17}$$

and

$$\begin{aligned} H_{X,Y}=&-\frac{1}{2}\left(\frac{\partial^2}{\partial X^2}+\frac{\partial^2}{\partial Y^2}\right)+\frac{1}{2}\left(X^2+Y^2\right) \\ &+\frac{g}{\sqrt{2}}\left[\delta\left(X\right)+\delta\left(\frac{X+\sqrt{3}Y}{2}\right)+\delta\left(\frac{X-\sqrt{3}Y}{2}\right)\right]. \end{aligned} \tag{3.18}$$

Hence, the wave function can be factorized as $\Psi\left(R,X,Y\right)=\phi\left(R\right)\psi\left(X,Y\right)$, which satisfy $H_R\phi\left(R\right)=E_R\phi\left(R\right)$ and $H_{X,Y}\psi\left(X,Y\right)=E_{X,Y}\psi\left(X,Y\right)$. The equation for $\phi\left(R\right)$ can be solved easily, so the main problem is solving the equation for $\psi\left(X,Y\right)$.

Since the system consists of identical bosonic atoms, the wave function should be unchanged under any permutation between x_1, x_2 and x_3. In the new coordinate system, R remains unchanged under any permutation, so it is

necessary for us to focus on $H_{X,Y}$ only. First, the effect of exchanging x_1 and x_2 in the new variables is:

$$\begin{pmatrix} X' \\ Y' \end{pmatrix} = \begin{pmatrix} -1 & 0 \\ 0 & 1 \end{pmatrix} \begin{pmatrix} X \\ Y \end{pmatrix}, \tag{3.19}$$

which represents a reflection against the Y axis. Secondly, the exchange in x_2 and x_3 gives

$$\begin{pmatrix} X' \\ Y' \end{pmatrix} = \begin{pmatrix} \frac{1}{2} & -\frac{\sqrt{3}}{2} \\ -\frac{\sqrt{3}}{2} & -\frac{1}{2} \end{pmatrix} \begin{pmatrix} X \\ Y \end{pmatrix}, \tag{3.20}$$

which represents a reflection against the line $\theta = 5\pi/6$. Finally, the exchange in x_1 and x_3 gives

$$\begin{pmatrix} X' \\ Y' \end{pmatrix} = \begin{pmatrix} \frac{1}{2} & \frac{\sqrt{3}}{2} \\ \frac{\sqrt{3}}{2} & -\frac{1}{2} \end{pmatrix} \begin{pmatrix} X \\ Y \end{pmatrix}, \tag{3.21}$$

which represents a reflection against the line $\theta = \pi/6$. Therefore, the original problem reduces to determining the eigenfunctions and eigenvalues for the $H_{X,Y}$ equation in the region $\pi/6 \leq \theta \leq \pi/2$.

3.2.2 Numerical simulation and results

In order to diagonalize the Hamiltonian for system of three or more interacting atoms, different numerical approaches have been developed by some authors. For examples, exact diagonalization [50], Quantum Monte Carlo [51] and the multiconfiguration time-dependent Hartree (MCTDH) method [42, 43, 52] with the help of relaxation method [53]. Among these, MCTDH is the most commonly used method for simulating few-atom system. However, MCTDH requires a large number of basis functions to give accurate results when the interaction is strong. Also, it is necessary to extrapolate the delta potential by a small-width Gaussian function [40].

In order to reduce the computational workload, we discretize the time independent Schrödinger's equation for $H_{X,Y}$ and apply the method of finite difference (FD) to solve it. Using FD, the delta potential between the atoms can be turned into boundary conditions for $\psi(X,Y)$, so Gaussian approximation is unnecessary. The detail for the method is included in Appendix A. Since we do not stick with any basis, the method can be applied equally well for strongly interacting systems. Apart from numerical approaches, Brouzos and Schmelcher [40] suggested that the relative wave function can be well approximated by the correlated pair wave function (CPWF). Later, we will compare our numerical results with them.

Using FD, we diagonalize $H_{X,Y}$ at different values of g. Due to the limitation in resources, the simulation was basically performed by an ordinary notebook. We used the software: Wolfram Mathematica 8 and HP Pavilion dv5 notebook which contains 4 GB RAM. The number of girds is 100 for each variable X and Y. As a result, the size of the Hamiltonian matrix for H_{XY} is 10000×10000. Fortunately, the matrix for the two-dimensional Schrödinger's equation is quite sparse. We then apply the command *SparseArray* in the Mathematica and finding the few lowest eigenvalues by using the inbuilt Arnoldi algorithm. Under this configuration, each diagonalization generally takes about $30 - 35$ seconds. Surely, the computational time depends on the computer. For checking of convergence, we have simulated the same system by using 150 girds for each variable on a PC with 8 GB RAM. In this case, the size of the Hamiltonian matrix is increased to 22500×22500. Using the same program and algorithm, the largest change to the energy in the range $g = 0$ to $g = 15$ is about 1 percent. For this larger matrix, each computation takes about $90 - 100$ seconds. We have compared our results explicitly with Fig. 2a in ref. [40]. Both of our results agree with each other.

For demonstration, we have plotted the energy spectrum for the system against the coupling strength and shown it in Fig. 3.8. It is observed that

the energy first increases and eventually saturate as the system transits from the weakly interacting limit to the tonks gas limit. Indeed, the feature for the energy spectrum can be understood easily. When the atoms are weakly interacting, the atoms can be approximated as three independent harmonic oscillators, which gives a ground state energy of $0.5 \times 3 = 1.5$. In the Tonks gas limit, the atoms behave as three independent spinless fermions. In this case, the atoms mimics the Pauli exclusion principle. As a result, the ground state energy for the system is $0.5 + 1.5 + 2.5 = 4.5$.

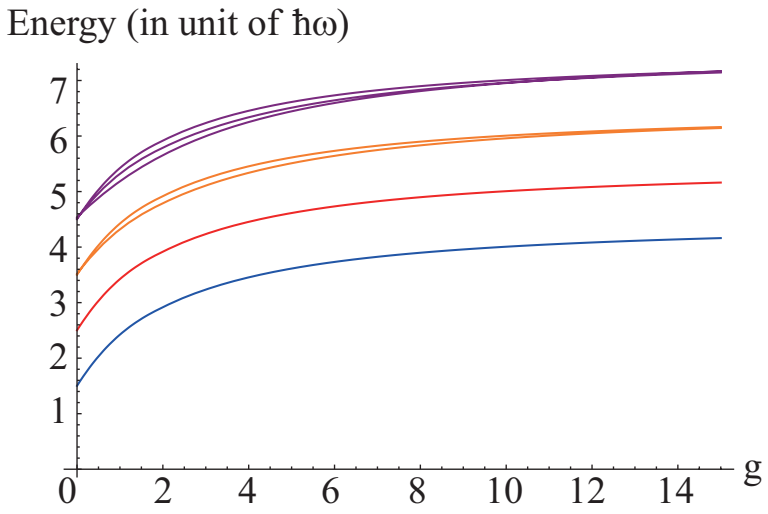

Figure 3.8: Energy spectrum for the three-atom system against g.

Apart from the ground state energy, energies for higher excited states have also been plotted. The splitting in the energy levels when g increases is the direct consequence from the interaction between the atoms. Eventually, the energy levels become nearly degenerate at the Tonks gas limit. Furthermore, the relative wave function $\psi(X, Y)$ obtained numerically at various values of g are shown in Fig. 3.9. Clearly, $\psi(X, Y)$ tends to separate into six symmetric pieces as g increases, which visualizes the symmetry for $H_{X,Y}$ and the effect from the boundary conditions due to the interaction. Here, the results for the ground state are shown only. Indeed, our numerical approach can be applied

to find the wave functions for the excited states also.

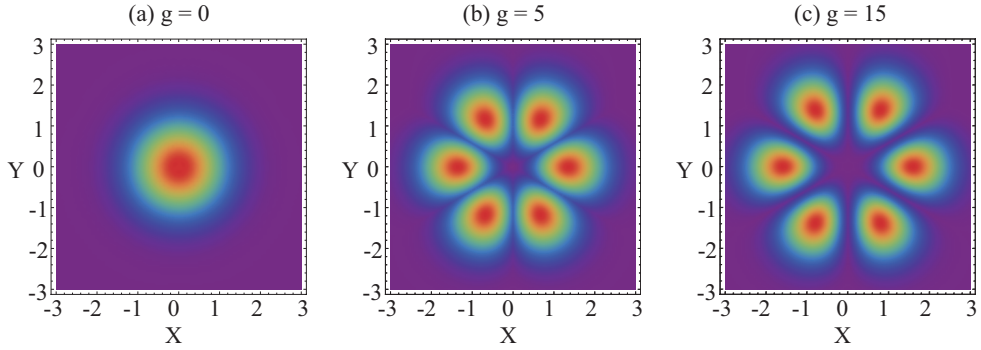

Figure 3.9: The relative wave functions $\psi(X, Y)$ obtained by FD.

3.2.3 Schmidt decomposition

Similar to the two-atom system, we evaluated the RSPDM for the system at different values of coupling strength. The result is shown in Fig. 3.10. Here, we observed similar features as in the two-atom case. However, the number of peaks at the Tonks gas limit is increased from two to three, which is a direct consequence from the increasing number of atoms. Generally, the number of peaks at the Tonks gas limit is the same as the number of atoms in the system [42] since the atoms are impenetrable and impossible to occupy the same position.

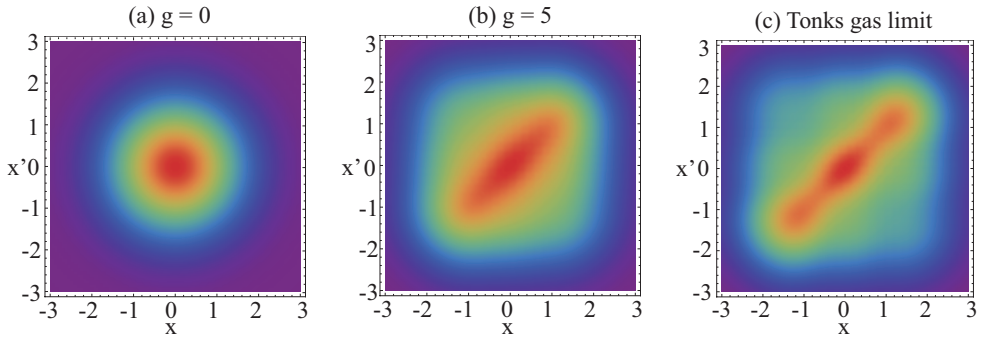

Figure 3.10: RSPDMs for the ground sate of the three-atom system.

Also, we performed the Schmidt decomposition on the wave function for the ground state of the system. To prevent confusion, it is reminded that the wave function here means $\Psi(x_1, x_2, x_3)$. For the present system, we define the Schmidt decomposition as

$$\Psi(x_1, x_2, x_3) = \sum_i \sqrt{\lambda_i} u_i(x_1) v_i(x_2, x_3). \tag{3.22}$$

The largest four Schmidt coefficients and their sum against the coupling strength are plotted in Fig. 3.11.

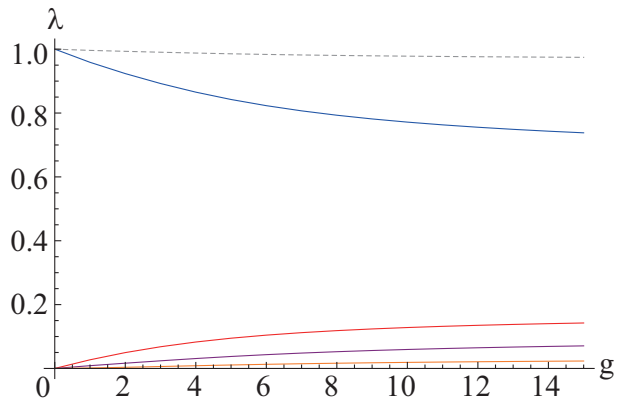

Figure 3.11: Largest four Schmidt coefficients (solid lines) and their sum (dashed line) for the ground state of the three-atom system.

From the figure, we see that the largest eigenvalue decreases as g increases. However, it decreases faster and the saturated value is smaller than the corresponding value in the two-atom system. In addition, the sum of the largest four Schmidt coefficients gives about 0.974 when $g = 15$, which is smaller than the two-atom system. Therefore, we conclude that four different Schmidt modes provide good approximation to the ground state of the three-atom system.

Furthermore, Fig. 3.12 and 3.13 show the most occupied Schmidt mode $u(x)$ and $v(x_2, x_3)$ at various values of g respectively. The purity and the entropy for the system, defined in (3.11) and (3.12) are shown in Fig. 3.14. As compared with Fig. 3.6 for the two-atom system, it is observed that the purity

for the present system decreases faster, whereas the entropy increase faster. These two results are expected since more Schmidt modes are necessary to describe the three-atom system.

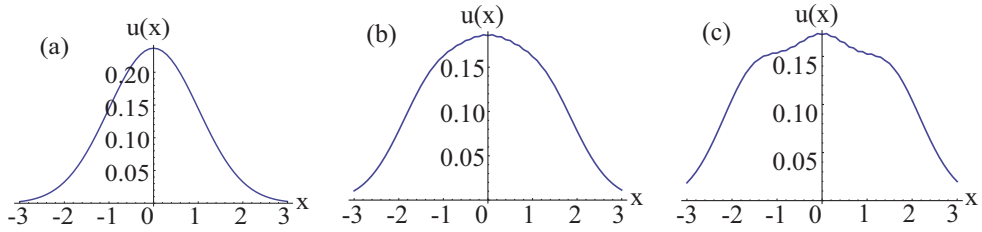

Figure 3.12: The most occupied Schmidt modes $u(x)$ for the ground state of the three-atom system when (a) $g = 0$, (b) $g = 5$ and (c) $g \to \infty$.

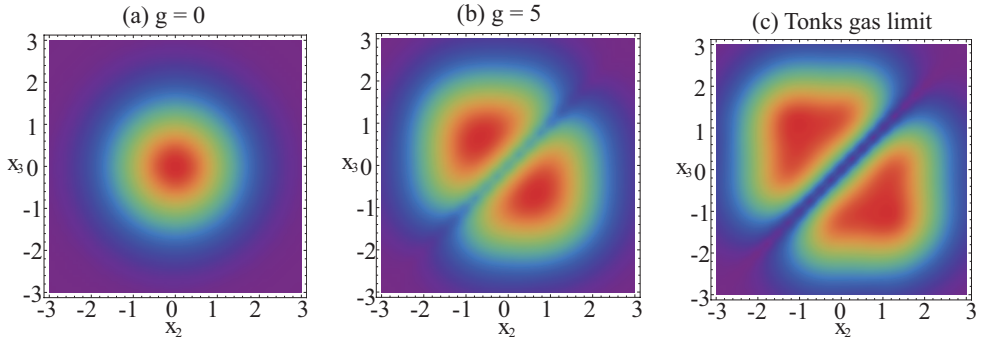

Figure 3.13: The most occupied Schmidt modes $v(x_2, x_3)$ for the ground state of the three-atom system.

Finally, we study the correlation between two atoms by evaluating the pair distribution function (PDF), which is defined in (2.24). The PDF for the ground state of the system for various values of g have been evaluated and the results are shown in Fig. 3.15.

3.2.4 Second order coherence function

Using the definition in (3.13), we evaluated the second order coherence function for the three-atom system. The results are shown in Fig. 3.16. Similar

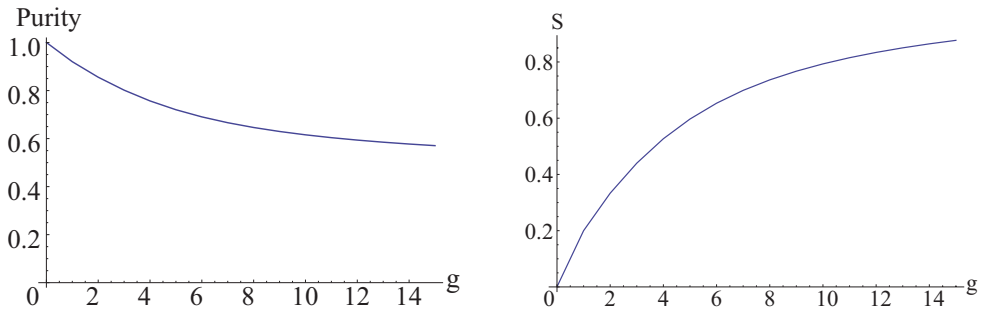

Figure 3.14: Purity (left) and the entropy (right) for the ground state of the three-boson system.

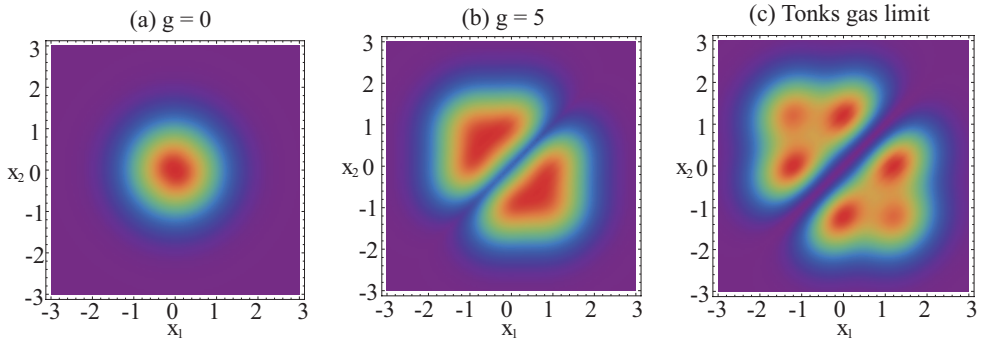

Figure 3.15: PDFs for the ground state of the three-boson system.

to the two-atom system, the result for the Tonks gas limit can also be evaluated analytically:

$$G^{(2)}(x_1, x_2) = \frac{6(x_1 - x_2)^2 (2x_1^2 + 2x_2^2 + 4x_1^2 x_2^2 + 8x_1 x_2 + 3)}{(3 + 4x_1^4)(3 + 4x_2^4)}. \tag{3.23}$$

3.3 Remark

In the previous discussion, the second order correlation function for the Tonks gas system with two atoms (3.14) and three atoms (3.23) have been evaluated analytically. Indeed, we have performed similar calculation for the system of four or five atoms. We list the results here and share the pattern we

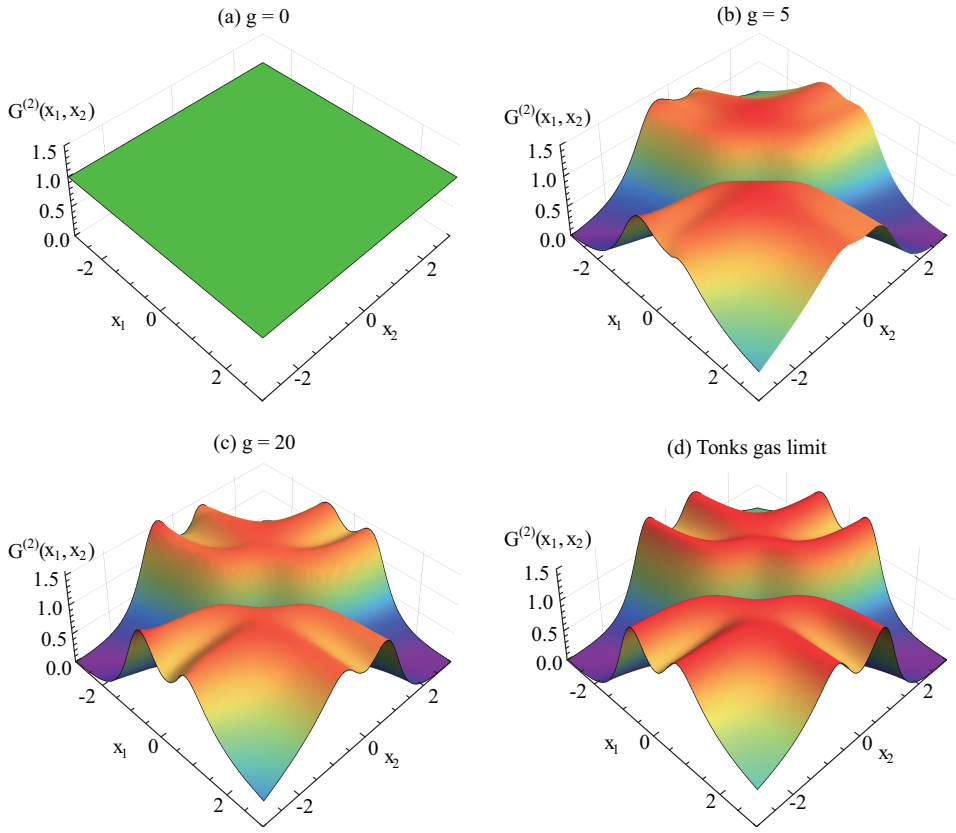

Figure 3.16: Second order coherence functions for three-atom system.

found. For the system of four atoms, we have

$$G^{(2)}(x_1, x_2) = \frac{8(x_1 - x_2)^2 f_4(x_1, x_2)}{(9 + 18x_1^2 - 12x_1^4 + 8x_1^6)(9 + 18x_2^2 - 12x_2^4 + 8x_2^6)} \tag{3.24}$$

with

$$\begin{aligned} f_4(x_1, x_2) = {} & 12x_1^4 + 12x_2^4 + 16x_1^4x_2^4 + 64x_1^3x_2^3 \\ & - 24x_1^2 - 24x_2^2 + 96x_1^2x_2^2 + 48x_1x_2 + 45. \end{aligned} \tag{3.25}$$

The maximum value for $G^{(2)}(x_1, x_2)$ is $4/3$ in this case. In addition, we have the analytical result for the system of five atoms:

$$G^{(2)}(x_1, x_2) = \frac{10(x_1 - x_2)^2 f_5(x_1, x_2)}{(45 + 120x_1^4 - 64x_1^6 + 16x_1^8)(45 + 120x_2^4 - 64x_2^6 + 16x_2^8)} \tag{3.26}$$

with

$$\begin{aligned} f_5(x_1,x_2) = {} & 72x_1^6 + 72x_2^6 + 64x_1^6x_2^6 - 96x_1^6x_2^4 - 96x_1^4x_2^6 \\ & + 144x_1^6x_2^2 + 144x_1^2x_2^6 - 384x_1^5x_2^3 - 384x1^3x2^5 \\ & + 384x_1^5x_2^5 + 288x_1^5x_2 + 288x_1x_2^5 - 180x_1^4 - 180x_2^4 \\ & + 1200x_1^4x_2^4 - 1080x_1^2x_2^4 - 1080x_1^4x_2^2 + 1920x_1^3x_2^3 \\ & - 1440x_1^3x_2 - 1440x_1x_2^3 + 90x_1^2 + 90x_2^2 + 2340x_1^2x_2^2 \\ & + 2520x_1x_2 + 675. \end{aligned} \tag{3.27}$$

I promise, this is the most horrible result in this thesis. The corresponding maximum value for $G^{(2)}(x_1,x_2)$ is 5/4. For demonstration, we plot the result for (3.24) and (3.26) in Fig. 3.17. From the results for two to five atoms, we conjecture that the maximum value for $G^{(2)}(x_1,x_2)$ with N atoms in the Tonks gas limit is $(N+1)/N$. If the conjecture is valid, the extreme limit $N \to \infty$ will give 1 to the maximum value.

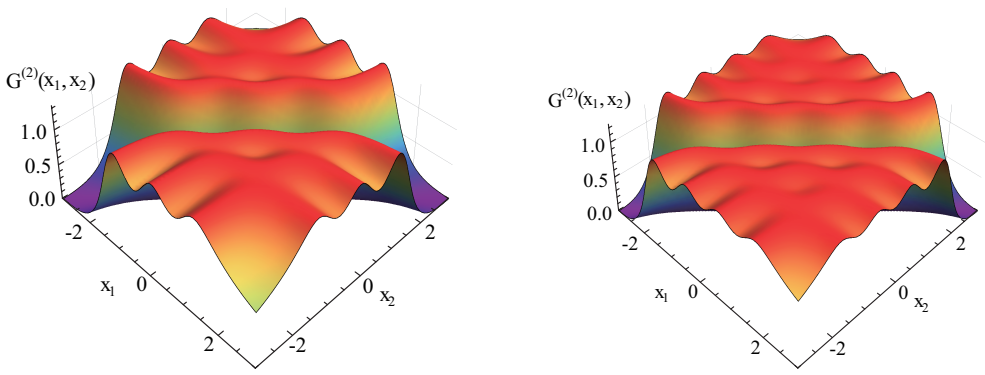

Figure 3.17: Second order coherence functions for the Tonks gas system with four (left) or five (right) atoms.

Chapter 4

An impurity atom immersed in a Tonks gas

In Chapter 2, it was pointed out that the ground state wave function for a system of Tonks gas is given by the Bose-Fermi mapping theorem. Later, Girardeau and Minguzzi [54] generalized the theorem to the system with mixture of Tonks gases, which is now known as the generalized Bose-Fermi mapping theorem.

In this chapter, we apply the generalized theorem to study the system of an impurity atom immersed in a background of Tonks gas. The interaction between the impurity and the background atom is assumed to be infinitely repulsive ($g \to \infty$). If both the atomic masses for the impurity and the background atoms are the same, it seems that the system under concerned can be reduced to a pure Tonks gas system with $N + 1$ atoms. However, we must think of the symmetrization for the wave functions carefully, so that we can really understand the differences between the two systems. For the pure Tonks gas system, the wave function must be symmetrized among all $N + 1$ atoms. However, the wave function is symmetrized among the N background atoms only for the present system. It is this important feature which makes the

two systems different. As a direct consequence, it is illegitimate to describe the spatial distribution for the impurity by directly quoting the single particle density (SPD) for the Tonks gas system.

Motivated by the above discussion, we focus on the spatial distribution for the impurity by evaluating its SPD after defining the quantity carefully. It is observed that the impurity atom localizes more due to the interaction with the Tonks gas. Specifically, we study the relationship between the degree of localization and the number of the background atoms. When the number is small, the SPD for the impurity atom can be obtained through numerical integration. Furthermore, it is found that the numerical results can be well approximated by Gaussian distributions if the impurity is placed at the middle of the system. Finally, we discuss the possible changes to the results if the impurity is placed at one side of the system.

4.1 System and Hamiltonian

The atomic masses of the background atoms and the impurity atom are denoted as m_B and m_I respectively. Here, we assume $m_B = m_I$. Also, we assume that all the background atoms and the impurity are trapped by the same harmonic potential with angular frequency ω. The positions of the background atoms and the impurity atom are labelled as $x_i\,(i = 1, 2, \cdots, N)$ and y respectively. Using the rescaled units defined in Chapter 3, the Hamiltonian for the system is

$$H = -\frac{1}{2}\left(\sum_{i=1}^{N}\frac{\partial^2}{\partial x_i^2} + \frac{\partial^2}{\partial y^2}\right) + \frac{1}{2}\left(\sum_{i=1}^{N} x_i^2 + y^2\right). \tag{4.1}$$

Due to the interaction, the wave function $\Psi\left(x_1, x_2, \cdots, x_N; y\right)$ must satisfy the boundary condition:

$$\Psi\left(x_1, x_2, \cdots, x_N; y\right) = 0, \quad \text{when } x_i = x_j \text{ and } x_i = y. \tag{4.2}$$

Also, the wave function must remain unchanged under any permutation between x_i and x_j.

Similar to the Tonks gas system, an $(N+1)\times(N+1)$ Slater determinant made up of the lowest $N+1$ eigenstates for the single harmonic oscillator is constructed:

$$\Psi_F = \frac{1}{\sqrt{(N+1)!}} \begin{vmatrix} \psi_0(x_1) & \psi_0(x_2) & \cdots & \psi_0(x_N) & \psi_0(y) \\ \psi_1(x_1) & \psi_1(x_2) & \cdots & \psi_1(x_N) & \psi_1(y) \\ \vdots & \vdots & \ddots & \vdots & \vdots \\ \psi_N(x_1) & \psi_N(x_2) & \cdots & \psi_N(x_N) & \psi_N(y) \end{vmatrix}. \tag{4.3}$$

Here, the importance for the conditions $m_B = m_I$ and equal trapping potential should be noticed. Suppose $m_B \neq m_I$, the background atoms and the impurity are not governed by the same single-particle Hamiltonian. In this case, the eigenfunctions for them are totally different, so the Slater determinant is no longer a correct solution to the mapped fermionic system.

Next, the improper symmetrization of the wave function is resolved by introducing the modified antisymmetric function [54]:

$$\mathcal{A}(x_1, x_2, \cdots x_N; y) = \prod_{1\leq i<j\leq N} \operatorname{sign}(x_j - x_i) \prod_{j=1}^{N} \operatorname{sign}(x_j - y). \tag{4.4}$$

Here, the first part of $\mathcal{A}$ restores the symmetry of the wave function when we exchange any two background atoms. However, exchanging x_i and y introduces a negative sign to the wave function due to the antisymmetry of the Slater determinant. This additional negative sign should not appear when we exchange distinguishable particles. Therefore, the second part of $\mathcal{A}$ is introduced to take care of this issue. Putting all arguments together, the wave function for the impurity-Tonks gas system is provided by the generalized Bose-Fermi mapping theorem:

$$\Psi_B(x_1, x_2, \cdots, x_N; y) = \mathcal{A}(x_1, x_2, \cdots, x_N; y)\, \Psi_F(x_1, x_2, \cdots, x_N; y). \tag{4.5}$$

The solution is valid for any configuration of x_i and y. The corresponding ground state energy for the system is

$$E_{\text{gs}} = \frac{1}{2} + \frac{3}{2} + \cdots + \frac{2N+1}{2} = \frac{(N+1)^2}{2}. \tag{4.6}$$

Clearly, the energy is the same as the system of $N+1$ non-interacting fermions, in which the particles need to obey Pauli's exclusion principle. Also, it is reminded that the energy is measured in unit of $\hbar\omega$.

4.2 Spatial distribution of the impurity

To study the spatial distribution of the impurity, we evaluate its SPD which is defined as

$$\rho(y) = \int_{\mathcal{M}} |\Psi_B(x_1, x_2, \cdots, x_N; y)|^2 \, \mathrm{d}x_1 \mathrm{d}x_2 \cdots \mathrm{d}x_N. \tag{4.7}$$

Here, $\mathcal{M}$ represents the region of the integration. When we wrote down the wave function of the system, we did not specify the configuration of x_i and y. Since we have no knowledge about the configuration, it is necessary for us to evaluate the integral throughout the entire space. Apart from a normalization factor, the corresponding result is the same as the SPD for the Tonks gas system in (2.23). However, this result cannot fully capture the real situation in experiments.

4.2.1 Experimental preparation

To understand the subtlety, the experimental procedures for preparing the system will be discussed briefly. Since the atomic masses for the impurity and the background atoms are required to be equal, same species of atoms must be used for both of them. In this case, the impurity atom can be created by the Raman process [55]. For example, Palzer *et al.* [36] trapped ^{87}Rb atoms in hybrid magnetic and optical potential. In order to create and identify

an impurity from the indistinguishable atoms, a $\pi/2$ radio frequency pulse resonant with $|F = 1, m_F = -1\rangle \rightarrow |F = 1, m_F = 0\rangle$ was applied. Due to the pulse, some atoms will be excited to a different hyperfine state, which serve as impurities to the system.

Suppose the impurity was initially created at the middle of the whole system, it cannot move aside due to its interaction with the background atoms. This peculiar feature sets constraints on the region of integration. In other words, $\mathcal{M}$ is confined as one of the portions for the entire space which depends on the initial configuration of the system.

4.2.2 Case 1: Impurity at the middle

Physically, it is expected that the quantum pressure exerting on the impurity by the background atoms should be the largest if the impurity is placed at the middle. This idea suggests that the impurity should be the most localized under this configuration. Therefore, we first assume $\mathcal{M} : x_1 < x_2 < \cdots < x_{N/2} < y < x_{N/2+1} < \cdots < x_N$.

Due to the irregularity in shape and the high dimension of $\mathcal{M}$, it is not a good idea for us to approximate the integral by trapezoidal rule or Simpson's rule. To evaluate (4.7) more effectively, the Monte-Carlo method provided in Wolfram Mathematica 8 is used. However, the calculation becomes time-consuming and the convergence drops quickly as N increases. For the present configuration, $N = 8$ is the best case we can do. Under this limitation, we plotted the numerical results from $N = 0$ to $N = 8$ (N must be even to achieve the prescribed condition) in Fig. 4.1. The case when $N = 0$ is plotted for emphasising the localization of impurity due to the interaction with the background atoms.

First, it is observed that the numerical results ensemble bell-shaped distributions with mean $\bar{y} = 0$. Also, the widths of the distributions when $N > 0$

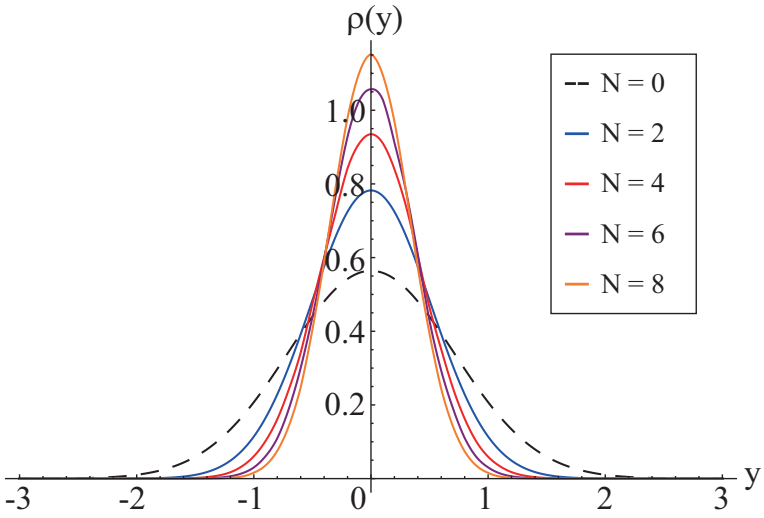

Figure 4.1: The SPDs for the impurity with different number of background atoms. Here, we consider the ground state of the system with the impurity at the middle.

are smaller and decrease as N increases. These observations suggest that the increase in the number of background atoms enhances the localization effect for the impurity, which is a direct consequence of the increase in the quantum pressure exerting on it. As a result, it is expected that the impurity should be strongly localized at $y = 0$ with an extremely small width when $N \to \infty$.

Gaussian approximation

Numerically, it is necessary for us to evaluate the integral in (4.7) for every value of y to obtain the SPD. However, the bell-shaped distributions in the numerical results motivate us to fit them by Gaussian distributions. Specifically, we fit the SPD at each value of N by using a Gaussian distribution with mean $\bar{y} = 0$ and variance $\sigma = \left[\sqrt{2\pi}\rho\left(0\right)\right]^{-1}$:

$$\rho\left(y\right) = \rho\left(0\right) \mathrm{Exp}\left[-\pi\rho^2\left(0\right) y^2\right]. \tag{4.8}$$

Here, it is necessary for us to evaluate $\rho(0)$ directly from (4.7) such that

$$\rho(0) = \int_{\mathcal{M}} |\Psi_B(x_1, x_2, \cdots, x_N; 0)|^2 \, \mathrm{d}x_1 \mathrm{d}x_2 \cdots \mathrm{d}x_N. \tag{4.9}$$

In order to check the validity of the approximation, we plot the numerical results and the corresponding fittings in Fig. 4.2.

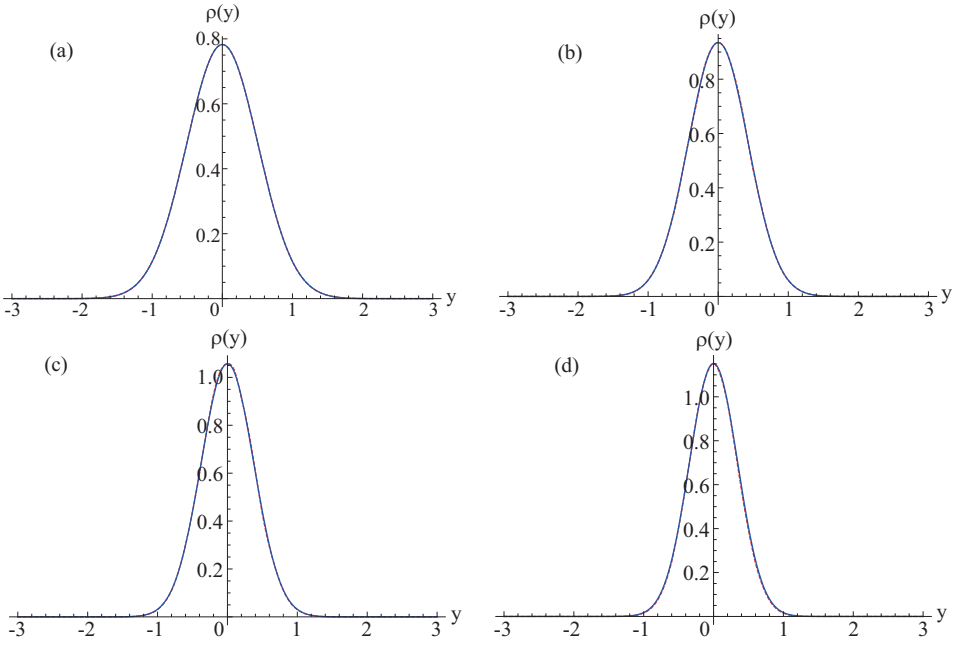

Figure 4.2: Comparison between the numerical results and the model for (a) $N = 2$, (b) $N = 4$, (c) $N = 6$ and (d) $N = 8$. The dotted lines and the solid lines correspond to the numerical results and the fitting respectively. It is reminded that the two sets of lines nearly coincide, so the dotted lines are difficult to visualize.

From the figure, it is clear that the numerical result and the fitting agree with each other well. To be more quantitative, we evaluate the fidelity of them. Denote the numerical result and the fitting as $\rho_{\mathrm{num}}(y)$ and $\rho_{\mathrm{fit}}(y)$ respectively, then the fidelity of them is defined as

$$\mathcal{F} = \int_{-\infty}^{\infty} \sqrt{\rho_{\mathrm{num}}(y) \, \rho_{\mathrm{fit}}(y)} \mathrm{d}y. \tag{4.10}$$

The results are summarized in Table. 4.1.

N	$\mathcal{F}$
2	0.99999
4	0.99997
6	0.99994

Table 4.1: Fidelity of the numerical result and the fitting for the SPD

Apart from possible tiny errors due to the Monte-Carlo integration, it is clear that the fidelities are very closed to one which suggests that the numerical results can be well approximated by using the Gaussian approximation in (4.8). Due to the good agreement as shown above, it is possible for us to just calculate $\rho(0)$ according to (4.9) and approximate $\rho(y)$ by (4.8), which reduces the computational workload dramatically. For example, we have evaluated $\rho(0)$ in (4.9) analytically from $N = 2$ to $N = 6$ and summarize the results in Table 4.2. For larger N, the analytic results cannot be provided by the software.

N	Analytic result for $\rho(0)$	σ
2	$2\pi^{-3/2} + \frac{3}{4}\pi^{-1/2}$	1.28
4	$\frac{16}{3}\pi^{-5/2} + \frac{125}{96}\pi^{-3/2} + \frac{45}{64}\pi^{-1/2}$	1.07
6	$\frac{2048}{135}\pi^{-7/2} + \frac{11809}{3600}\pi^{-5/2} + \frac{35827}{30720}\pi^{-3/2} + \frac{175}{256}\pi^{-1/2}$	0.95

Table 4.2: Analytical results for $\rho(0)$ and the corresponding width σ when $N = 2$, $N = 4$ and $N = 6$ by Mathematica

From the table, we conjecture that $\rho(0)$ is given by the series:

$$\rho(0) = \sum_{n=0}^{N/2} c_n \pi^{-\frac{2n+1}{2}}. \tag{4.11}$$

However, the calculation of c_n becomes impractical at larger value of N, which constrains our studies on background with few atoms only.

Purity of the impurity atom

To study the correlation between the impurity and the background atoms, we have evaluated the RSPDM for the impurity. Due to the computational limit, the cases for $N = 2$ and $N = 4$ are evaluated. The results are shown in Fig. 4.3. It is observed that when $N = 4$, the RSPDM for the impurity is more squeezed as compared with the case of $N = 2$.

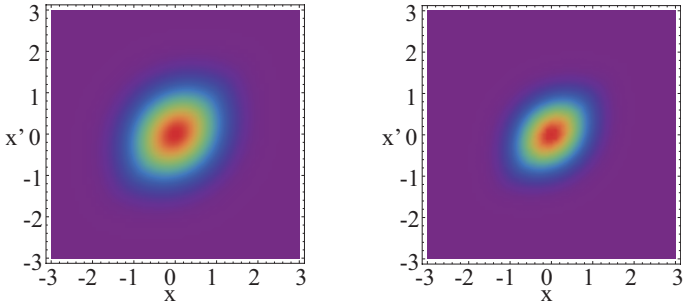

Figure 4.3: Density plots of the RSPDMs for the impurity when $N = 2$ (left) and $N = 4$ (right).

To understand the correlation between the impurity and the background atoms, we perform the Schmidt decomposition to obtain the Schmidt coefficients λ and the purity from the RSPDM. The results are summarized in Table. 4.3. It is observed that both λ_0 and the purity decrease when the number of background atoms increases, which directly shows that the impurity is more correlated with the background atoms as N increases.

N	λ_0	λ_1	λ_2	Purity
2	0.869	0.100	0.020	0.765
4	0.833	0.124	0.026	0.711

Table 4.3: The three largest Schmidt coefficients and the purity for the impurity atom when $N = 2$ and $N = 4$

4.2.3 Case 2: Impurity at the side

Previously, we mentioned that the spatial distribution for the impurity depends on the position of the impurity. In order to study the differences, we consider the case when the impurity is placed at the right-hand side of the system. Mathematically, we have $\mathcal{M} : x_1 < x_2 < \cdots < x_N < y$. The SPD for the impurity is shown in Fig. 4.4.

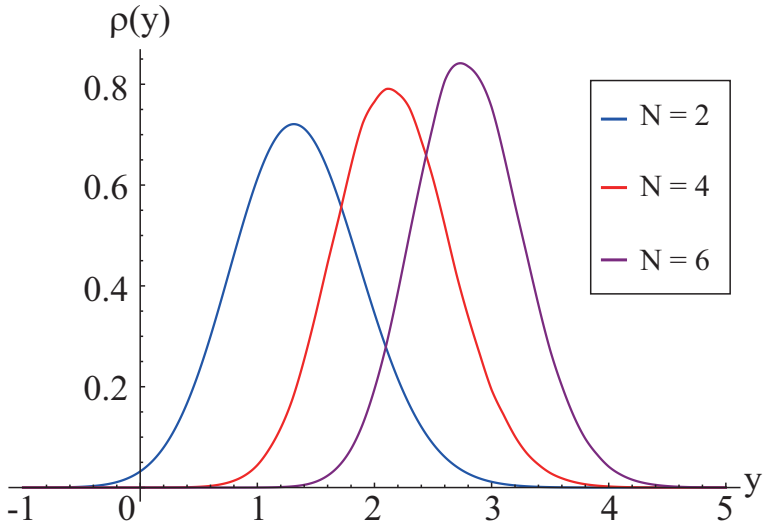

Figure 4.4: The SPDs for the impurity with different number of background atoms. Here, we consider the ground state of the system with the impurity at the right-hand side.

From the figure, we notice that the distributions are slightly left-skewed. It is because the quantum pressure exerting on the impurity is contributed from the left-hand side only. If we compare the results with Fig. 4.1, it is observed that the localization effect in the present configuration is weaker, which agrees with the prediction we made before the numerical calculation. Indeed, the configuration of the system can also affect the energy and the wave function if the background atoms are non-interacting, which is discussed in Appendix B.

4.3 Remark

To have a deeper understanding for the Gaussian approximation, we have evaluated (4.7) analytically when $N = 2$. The result is

$$\begin{aligned}\rho(y) =& \frac{4(2-y^2)\,\mathrm{Exp}(-3y^2) + 8\sqrt{\pi}y(1-y^2)\,\mathrm{Exp}(-2y^2)\,\mathrm{Erf}(y)}{4\pi^{3/2}} \\ &+ \frac{\pi\mathrm{Exp}(-y^2)(4y^4+3)\left[1-\mathrm{Erf}^2(y)\right]}{4\pi^{3/2}}.\end{aligned} \tag{4.12}$$

Here, it is clear that the SPD is much more complicated. However, the Gaussian approximation agrees with the results well and simplifies the problem dramatically, so it is suggestive for us to include it in the thesis.

Chapter 5

Self-localization of an impurity atom in a BEC

In Chapter 4, the spatial distribution for an impurity atom immersed in a harmonically trapped Tonks gas was studied. In that case, the localization for the impurity atom was not purely induced by the atom-atom interaction since all atoms were harmonically trapped. For systems without trapping potential, Cucchietti and Timmermans [56] first pointed out the possibility for self-localization of an untrapped impurity atom immersed in a three-dimensional Bose-Einstein condensate. Through the interaction, the impurity atom distorts the distribution of the surrounding condensate, such that an effective trapping potential for the impurity atom can be produced. Later, Sacha and Timmermans [57] shown that the same process is possible in one-dimensional systems also. In this case, self-localization occurs whenever the interaction between the impurity and the condensate atoms is non-zero [58]. This is different from the two-dimensional and three-dimensional cases, in which the process can occur only when the interaction between the impurity and the condensate exceeds a critical value [58].

In this chapter, we focus on the self-localization of an impurity atom immersed in a one-dimensional condensate. Two different approaches are used. For the first approach, we linearize the coupled Gross-Pitaevskii equations and apply the variational principle to approximate the impurity wave function. The optimal width for the wave function against the trapping parameter is obtained [58]. To understand the system deeper, we use a different trial wave function suggested by the analytic solution in [57] for comparison.

Furthermore, the distortion of the condensate can be interpreted as Bogoliubov excitations. In addition, it was suggested that the interaction between the impurity atom and the Bogoliubov excitations can be described by the Fröhlich polaron Hamiltonian [59, 60, 61, 62]. From the Hamiltonian, we write the distortion as a product of coherent states. Particularly, we obtain an approximated formula for the coherent amplitudes when $ky \ll 1$. Finally, the validity of the product form solution is discussed in Appendix D.

5.1 System and Hamiltonian

The system consists of an impurity atom immersed in a one-dimensional Bose-Einstein condensate. The masses of the condensate atom and the impurity atom are denoted as m_B and m_I respectively. The interaction between the condensate atoms is modelled by the Dirac delta potential $g_{BB}\delta\left(x_j - x_i\right)$, and the interaction between the impurity atom and the condensate atom is modelled by $g_{BI}\delta\left(y - x_i\right)$. The Hamiltonian of the system is

$$\begin{aligned}\hat{H} = &\int \hat{\psi}^\dagger\left(x\right)\left[-\frac{\hbar^2}{2m_B}\frac{d^2}{dx^2} + \frac{g_{BB}}{2}\hat{\psi}^\dagger\left(x\right)\hat{\psi}\left(x\right)\right]\hat{\psi}\left(x\right)\mathrm{d}x \\ &+ \int \hat{\phi}^\dagger\left(x\right)\left(-\frac{\hbar^2}{2m_I}\frac{d^2}{dx^2}\right)\hat{\phi}\left(x\right)\mathrm{d}x \\ &+ g_{BI}\int \hat{\psi}^\dagger\left(x\right)\hat{\psi}\left(x\right)\hat{\phi}^\dagger\left(x\right)\hat{\phi}\left(x\right)\mathrm{d}x. \end{aligned} \tag{5.1}$$

Here, $\hat{\psi}(x)$ and $\hat{\phi}(x)$ stand for the field operators for the condensate atom and the impurity atom respectively.

Under the product form approximation, the wave function for the system is assumed to be [56, 57, 61]:

$$\Psi(y; x_1, x_2, \cdots, x_N) = \phi(y) \prod_{i=1}^{N} \nu(x_i). \tag{5.2}$$

Here, $\phi(y)$ and $\nu(x_i)$ stand for the single particle wave functions for the impurity atom and the condensate atom respectively. The expectation value of (5.1) under (5.2) is

$$\begin{aligned} H = &\int \psi^*(x) \left[-\frac{\hbar^2}{2m_B} \frac{d^2}{dx^2} \psi(x) \right] \mathrm{d}x + \int \phi^*(x) \left[-\frac{\hbar^2}{2m_I} \frac{d^2}{dx^2} \phi(x) \right] \mathrm{d}x \\ &+ \frac{g_{BB}}{2} \int |\psi(x)|^4 \mathrm{d}x + g_{BI} \int |\psi(x)|^2 |\phi(x)|^2 \mathrm{d}x. \end{aligned} \tag{5.3}$$

Here, we have defined $\psi(x) = \sqrt{N}\nu(x)$ to represent the condensate wave function. Therefore, the normalization conditions are

$$\int |\psi(x)|^2 \mathrm{d}x = N \quad \text{and} \quad \int |\phi(x)|^2 \mathrm{d}x = 1. \tag{5.4}$$

Upon minimizing (5.3) with respect to $\psi(x)$ and $\phi(x)$, we obtain the coupled Gross-Pitaevskii equations for the system:

$$\left[-\frac{\hbar^2}{2m_B} \frac{d^2}{dx^2} + g_{BB}|\psi(x)|^2 + g_{BI}|\phi(x)|^2 \right] \psi(x) = \mu_B \psi(x), \tag{5.5}$$

$$\left[-\frac{\hbar^2}{2m_I} \frac{d^2}{dx^2} + g_{BI}|\psi(x)|^2 \right] \phi(x) = E_I \phi(x). \tag{5.6}$$

Here, μ_B and E_I are the chemical potentials for the condensate and the impurity respectively. The introduction of μ_B ensures the conservation of the condensate atoms number.

5.2 Linearization of equations

We write the condensate wave function as

$$\psi(x) = \sqrt{\rho} + \delta\psi(x), \tag{5.7}$$

where ρ is the number density of the condensate and $\delta\psi(x)$ stands for the distortion of the condensate due to the impurity-condensate interaction. Provided that

$$\left|\frac{\delta\psi(x)}{\sqrt{\rho}}\right| \ll 1, \tag{5.8}$$

it is possible for us to linearize (5.5) by keeping terms up to first order in $\delta\psi(x)$. The corresponding equations [57] are

$$\left(-\frac{\hbar^2}{2m_B}\frac{d^2}{dx^2} + 2g_{BB}\rho\right)\delta\psi(x) = -g_{BI}\sqrt{\rho}\phi^2(x), \tag{5.9}$$

$$\left[-\frac{\hbar^2}{2m_I}\frac{d^2}{dx^2} + 2g_{BI}\sqrt{\rho}\delta\psi(x)\right]\phi(x) = E_I'\phi(x), \tag{5.10}$$

with the assumption that $\delta\psi(x)$ and $\phi(x)$ are real. Here, we have defined $E_I' = E_I - g_{BI}\rho$ and $\mu_B = g_{BB}\rho$.

The general solution to the first equation in (5.9) is given by

$$\delta\psi(x) = -\frac{m_B g_{BI}\sqrt{\rho}\chi}{2\hbar^2}\int \phi^2(y)\, e^{-2|x-y|/\chi}\mathrm{d}y. \tag{5.11}$$

Here, χ stands for the healing length of the condensate, which is defined as

$$\chi = \frac{\hbar}{\sqrt{m_B g_{BB}\rho}}. \tag{5.12}$$

Substituting (5.11) into the second equation in (5.9), a self-consistent equation for the impurity wave function can be obtained [57]:

$$\left[-\frac{\hbar^2}{2m_I}\frac{d^2}{dx^2} - \frac{g_{BI}^2\rho m_B\chi}{\hbar^2}\int \phi^2(y)\, e^{-2|x-y|/\chi}\mathrm{d}y\right]\phi(x) = E_I'\phi(x). \tag{5.13}$$

From (5.13), it is observed that the impurity self-interacts with itself through an attractive exponential interaction mediated by the condensate. Analytically, it is difficult to solve (5.13) for general cases, but particular solutions do exist [57]. When the number density of the condensate satisfies

$$\rho = \frac{m_I^2 g_{BI}^4}{36\hbar^2 m_B g_{BB}^3}, \tag{5.14}$$

the distortion of the condensate and the impurity wave function are given by

$$\delta\psi(x) = -\sqrt{\frac{3}{8\chi}\left(\frac{m_B}{m_I}\right)}\operatorname{sech}^2\left(\frac{x}{\chi}\right),$$
$$\phi(x) = \sqrt{\frac{3}{4\chi}}\operatorname{sech}^2\left(\frac{x}{\chi}\right), \tag{5.15}$$

which suggest that the impurity self-localizes with a width equals to the healing length of the condensate.

5.3 First approach: Variational principle

For systems with conditions different from (5.14), the particular solution in (5.15) cannot be used. To study the self-localization systematically, Bruderer *et al.* [58] used the variational principle and introduced the following rescaled units:

$$\tilde{x} = \frac{x}{\chi}, \quad \delta\tilde{\psi} = \frac{\delta\psi}{\sqrt{\rho}}, \quad \tilde{\phi} = \sqrt{\chi}\phi. \tag{5.16}$$

Using the rescaled units, the equation for the impurity wave function in (5.13) becomes

$$\left[-\frac{\alpha}{2}\frac{d^2}{d\tilde{x}^2} - \beta^2\gamma\int\tilde{\phi}^2(\tilde{y})\,e^{-2|\tilde{x}-\tilde{y}|}\mathrm{d}\tilde{y}\right]\tilde{\phi}(\tilde{x}) = \frac{E_I'}{g_{BB}\rho}\tilde{\phi}(\tilde{x}), \tag{5.17}$$

with the dimensionless parameters defined as

$$\alpha = \frac{m_B}{m_I}, \quad \beta = \frac{g_{BI}}{g_{BB}}, \quad \gamma = \frac{1}{\rho\chi}. \tag{5.18}$$

From (5.17), the energy for the system is given by $E = E_{\text{kin}} + E_{\text{def}}$ with

$$E_{\text{kin}} = \int\tilde{\phi}(\tilde{x})\left[-\frac{\alpha}{2}\frac{d^2}{d\tilde{x}^2}\tilde{\phi}(\tilde{x})\right]\mathrm{d}\tilde{x},$$
$$E_{\text{def}} = -\frac{\beta^2\gamma}{2}\int\tilde{\phi}(\tilde{x})\,e^{-2|\tilde{x}-\tilde{x}'|}\tilde{\phi}(\tilde{x}')\,\mathrm{d}\tilde{x}\mathrm{d}\tilde{x}'. \tag{5.19}$$

Here, E_{kin} represents the kinetic energy of the impurity atom, whereas E_{def} represents the interaction energy between the impurity and the deformation of the condensate. It is possible for an optimal width to exist such that E is minimized and the value of E is smaller than 0.

5.3.1 Gaussian trial wave function

First, a Gaussian trial wave function with width σ (in unit of healing length) is assumed:

$$\tilde{\phi}\left(\tilde{x}\right) = \left(\frac{1}{\pi\sigma^2}\right)^{1/4} e^{-\frac{\tilde{x}^2}{2\sigma^2}}. \tag{5.20}$$

Then, we have E given explicitly by [58]

$$E = \frac{\alpha}{4\sigma^2} - \frac{\beta^2\gamma}{2} e^{2\sigma^2} \mathrm{Erfc}\left(\sqrt{2}\sigma\right), \tag{5.21}$$

where $\mathrm{Erfc}\left(x\right)$ stands for the complementary error function [46]. Minimizing (5.21) with respect to σ, we obtain the transcendental equation:

$$\sqrt{\frac{2}{\pi}}\zeta - \frac{1}{2\sigma^3} - 2\zeta\sigma e^{2\sigma^2} \mathrm{Erfc}\left(\sqrt{2}\sigma\right) = 0. \tag{5.22}$$

Here, it can be concluded that the width of the impurity wave function depends on the trapping parameter ζ only, which is defined as

$$\zeta = \frac{\beta^2\gamma}{\alpha}. \tag{5.23}$$

In order to study how the degree of self-localization varies against the trapping parameter, (5.22) is solved at different values of ζ. At the same time, $\delta\tilde{\psi}\left(\tilde{x}\right)$ is obtained from (5.11) (with proper rescaling). The corresponding results are fitted with Gaussian distributions with undetermined widths. For comparison, both results are shown in Fig. 5.1.

It can be observed that both the widths for the impurity wave function and the distortion decrease monotonically as the trapping parameter. There are two other important features to be noticed. First, $\sigma = \sqrt{2\pi}/\zeta$ when ζ tends to zero asymptotically [58]. Secondly, we find that the width for the impurity wave function is approximately half of the width for the distortion at the large ζ limit.

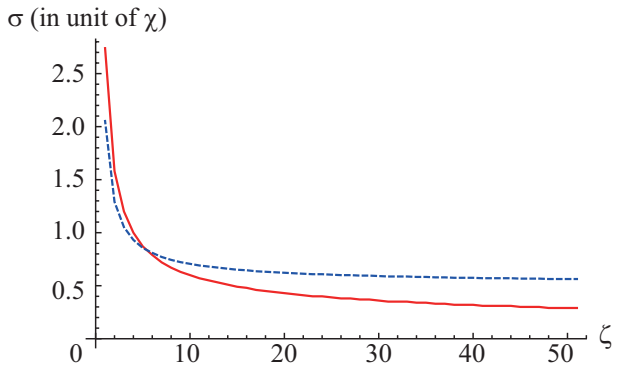

Figure 5.1: The widths of the impurity wave function (red solid line) and the distortion (blue dashed line) against ζ defined in (5.23) with Gaussian trial wave functions.

5.3.2 Hyperbolic secant trial wave function

Although the self-localization for the impurity was studied by using Gaussian trial wave function in [58], the particular solution in (5.15) suggests that the impurity wave function maybe better approximated by hyperbolic secant function. Therefore, we consider the following trial wave function:

$$\tilde{\phi}\left(\tilde{x}\right) = \sqrt{\frac{3}{4\sigma}}\mathrm{sech}^2\left(\frac{\tilde{x}}{\sigma}\right). \tag{5.24}$$

Using (5.24), we minimize E again and show the corresponding results in Fig. 5.2. We find that the widths for the impurity wave function and the distortion are the same at $\zeta = 6$ only, which is exactly the trapping parameter for (5.14) to hold.

Denote the energies from the Gaussian trial wave function and the hyperbolic secant trial wave function as E_1 and E_2 respectively, we evaluate $\left(E_2 - E_1\right)/E_2 \times 100\%$ and show the results against the trapping parameter in Fig. 5.3. Since the energy for the system is negative, the percentage difference should be positive if $E_2 < E_1$.

Here, we observe that the energy is smaller if the hyperbolic secant trial wave functions are used. From the particular solution and the comparison

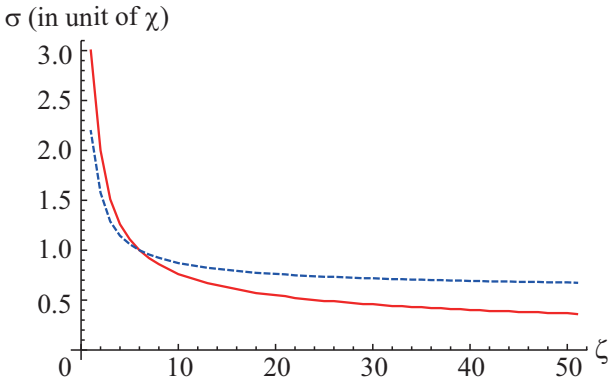

Figure 5.2: The widths of the impurity wave function (red solid line) and the distortion (blue dashed line) against the trapping parameter defined in (5.23) with hyperbolic secant trial wave functions.

between E_1 and E_2, we conclude that the impurity wave function is better described by (5.24). However, the difference in the energies is smaller than 3% when $\zeta > 1$. Since the calculation is much more convenient if the Gaussian trail wave functions are used, so we use them in Chapter 6.

5.4 Second approach: Fröhlich polaron Hamiltonian

After obtaining $\phi(x)$ from the variational principle, we can obtain $\delta\psi(x)$ from (5.11). By expanding $\delta\psi(x)$ in modes of quasi-particles, we have

$$\delta\psi(x) = \sum_{k\neq 0} Z_k \left(u_k \frac{e^{-ikx}}{\sqrt{l}} - v_k \frac{e^{ikx}}{\sqrt{l}} \right), \tag{5.25}$$

where u_k and v_k were defined in (2.51). Then, the coherent amplitudes Z_k are given by

$$Z_k = \int \delta\psi(x) (u_k + v_k) \frac{e^{-ikx}}{\sqrt{l}} \mathrm{d}x. \tag{5.26}$$

We plot Z_k (red dotted lines) for various values of ζ in Fig. 5.4. Here, the wave number k is in unit of χ^{-1} and Z_k are rescaled properly according to (5.16).

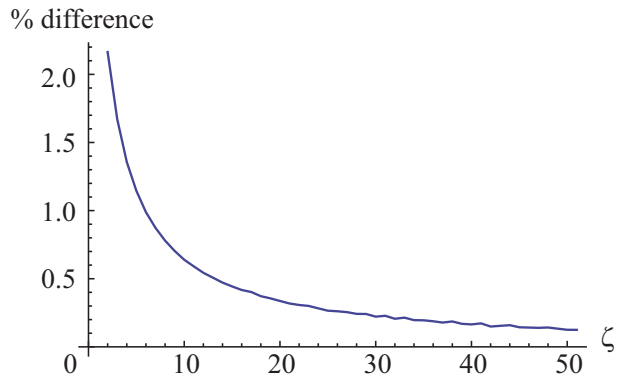

Figure 5.3: Percentage difference in the energies by using Gaussian trial wave functions and hyperbolic secant trial wave functions.

Generally, it is difficult to obtain the analytical form for Z_k. In order to obtain an approximated expression for Z_k, we study the system by considering the Fröhlich polaron Hamiltonian [59, 60, 61, 62]:

$$\hat{H}_{\text{pol}} = \frac{\hat{p}^2}{2m_I} + \sum_{k\neq 0} \xi(k)\, \hat{c}_k^\dagger \hat{c}_k + \sum_{k\neq 0} \frac{g_{BI}\sqrt{N}}{l} \sqrt{\frac{\epsilon(k)}{\xi(k)}} \left(e^{ik\hat{y}} \hat{c}_k + e^{-iky} \hat{c}_k^\dagger \right), \quad (5.27)$$

which is derived in Appendix C. It is reminded that $\epsilon(k)$ and $\xi(k)$ were defined in Chapter 2.

The state for the system is assumed to be factorized:

$$|\Psi\rangle = |\phi(y)\rangle \otimes \prod_k |Z_k\rangle\,, \quad (5.28)$$

with the Bogoliubov excitations for the condensate written as a product of coherent states. Here, we assume Z_k to be real. Then, we have

$$\begin{aligned} \langle \hat{H}_{\text{pol}} \rangle = \langle \phi(y)| \frac{\hat{p}^2}{2m_I} |\phi(y)\rangle + \sum_{k\neq 0} \xi(k)\, Z_k^2 \\ + 2 \sum_{k\neq 0} \frac{g_{BI}\sqrt{N}}{l} \sqrt{\frac{\epsilon(k)}{\xi(k)}} Z_k \cos ky. \end{aligned} \quad (5.29)$$

When $ky \ll 1$, we have $\cos ky \approx 1$ and (5.29) becomes

$$\langle \hat{H}_{\text{pol}} \rangle \approx \langle \phi(y)| \frac{\hat{p}^2}{2m_I} |\phi(y)\rangle + \sum_{k\neq 0} \left[\xi(k)\, Z_k^2 + \frac{2g_{BI}\sqrt{N}}{l} \sqrt{\frac{\epsilon(k)}{\xi(k)}} Z_k \right]. \quad (5.30)$$

Therefore,

$$Z_k \approx -\frac{g_{BI}\sqrt{N}}{l}\sqrt{\frac{\epsilon\left(k\right)}{\xi^3\left(k\right)}} \tag{5.31}$$

for $\langle \hat{H}_{\rm pol} \rangle$ to be minimized. The results from (5.26) and (5.31) should agree with each other when $ky \ll 1$. Also, they should agree with each other for a larger range of k when ζ is large since σ is monotonic decreasing against ζ. We plot the results from (5.31) (solid lines) for various values of ζ in Fig. 5.4 to check the validity of the approximation.

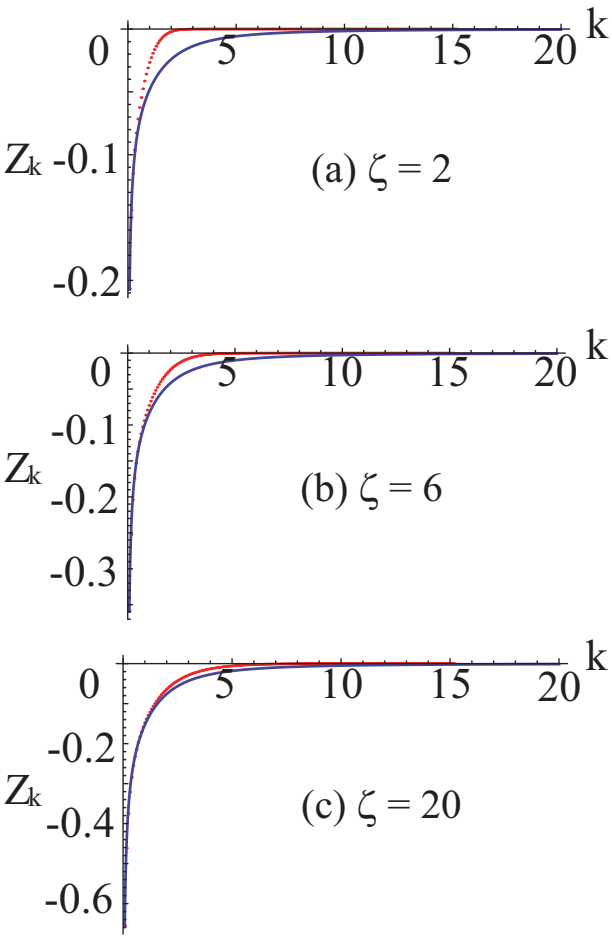

Figure 5.4: Z_k from (5.26) (dotted lines) and (5.31) (solid lines) at various values of ζ.

Chapter 6

Dynamics of an impurity atom in a BEC

In chapter 5, we have demonstrated that an untrapped impurity atom immersed in a Bose-Einstein condensate can become self-localized with a finite width, depending solely on the trapping parameter ζ. Apart from studying the system at equilibrium, the expansion of an initially localized impurity atom was studied experimentally [63]. It was observed that the impurity atom underwent breathing oscillation. Some authors [64, 65] have tried to explain the results theoretically.

In this chapter, we investigate a dynamical problem in which the initial wave function of the impurity atom has a width larger than its equilibrium value given by (5.22). Due to the interaction, the impurity atom exchanges energy with the condensate and reaches the equilibrium eventually. To describe the dynamics, we derive an effective generalized Langevin equation for the system by applying the time-dependent variational principle. By solving the Langevin equation, we successfully predict the period of the oscillation and the damping rate of the width. Furthermore, we numerically simulate the dynamics for the system and observe that phonon pulses are emitted during

the oscillation.

6.1 Effective generalized Langevin equation

With the same notations defined in Chapter 5, the Lagrangian density for the system is given by,

$$\begin{aligned}\mathcal{L} =&\frac{i\hbar}{2}\left(\psi^*\frac{\partial\psi}{\partial t}-\psi\frac{\partial\psi^*}{\partial t}\right)-\frac{\hbar^2}{2m_B}\left|\nabla\psi\right|^2-\frac{g_{BB}}{2}\left|\psi\right|^4+\mu_B\left|\psi\right|^2\\&+\frac{i\hbar}{2}\left(\phi^*\frac{\partial\phi}{\partial t}-\phi\frac{\partial\phi^*}{\partial t}\right)-\frac{\hbar^2}{2m_I}\left|\nabla\phi\right|^2-g_{BI}\left|\psi\right|^2\left|\phi\right|^2,\end{aligned}\tag{6.1}$$

with μ_B being the chemical potential for the condensate.

Next, we write

$$\psi\left(x,t\right)=\sqrt{\rho}+\delta\psi\left(x,t\right).\tag{6.2}$$

By keeping terms up to second order in $\psi\left(x,t\right)/\sqrt{\rho}$, we obtain the linearized Lagrangian density:

$$\begin{aligned}\mathcal{L} =&\frac{i\hbar}{2}\left(\delta\psi^*\frac{\partial}{\partial t}\delta\psi-\delta\psi\frac{\partial}{\partial t}\delta\psi^*\right)-\frac{\hbar^2}{2m_B}\left|\nabla\left(\delta\psi\right)\right|^2\\&+\frac{i\hbar}{2}\left(\phi^*\frac{\partial\phi}{\partial t}-\phi\frac{\partial\phi^*}{\partial t}\right)-\frac{\hbar^2}{2m_I}\left|\nabla\phi\right|^2\\&-\frac{g_{BB}\rho}{2}\left[\left(\delta\psi\right)^2+\left(\delta\psi^*\right)^2+2\left(\delta\psi\right)\left(\delta\psi^*\right)\right]\\&-g_{BI}\left(\rho+\sqrt{\rho}\delta\psi+\sqrt{\rho}\delta\psi^*\right)\left|\phi\right|^2,\end{aligned}\tag{6.3}$$

where $\mu_B=g_{BB}\rho$ has been used. We approximate the impurity wave function as Gaussian:

$$\phi\left(x,t\right)=\left(\frac{1}{\sqrt{\pi}\sigma\left(t\right)}\right)^{1/2}e^{-\frac{x^2}{2\sigma^2(t)}+i\beta(t)x^2},\tag{6.4}$$

with $\sigma\left(t\right)$ and $\beta\left(t\right)$ being the time-dependent variational parameters, specifying the width and the quadratic phase modulation of the impurity wave function respectively.

Using the time-dependent variational principle [66, 67], the action $S = \int \mathcal{L} \mathrm{d}x\mathrm{d}t$ is minimized with respect to the variational parameters. Substituting (6.4) into (6.3) and integrate over x, we obtain the Lagrangian for the system:

$$\begin{aligned} L = & \int \frac{i\hbar}{2}\left(\delta\psi^* \frac{\partial}{\partial t}\delta\psi - \delta\psi \frac{\partial}{\partial t}\delta\psi^*\right) \mathrm{d}x - \int \frac{\hbar^2}{2m_B} \left|\nabla\left(\delta\psi\right)\right|^2 \mathrm{d}x \\ & - \int \frac{g_{BB}\rho}{2}\left[\left(\delta\psi\right)^2 + \left(\delta\psi^*\right)^2 + 2\left(\delta\psi\right)\left(\delta\psi^*\right)\right] \mathrm{d}x \\ & - \frac{g_{BI}\sqrt{\rho}}{\sqrt{\pi}\sigma\left(t\right)} \int \left(\delta\psi + \delta\psi^*\right) e^{-\frac{x^2}{\sigma^2(t)}} \mathrm{d}x \\ & - \frac{\hbar}{2}\sigma^2\left(t\right)\dot{\beta}\left(t\right) - \frac{\hbar^2}{4m_I\sigma^2\left(t\right)}\left[1 + 4\beta^2\left(t\right)\sigma^4\left(t\right)\right]. \end{aligned} \tag{6.5}$$

Then, the equations for the variational parameters are obtained by the Euler-Lagrange equations:

$$\frac{d}{dt}\left(\frac{\partial L}{\partial \dot{q}_j}\right) = \frac{\partial L}{\partial q_j}, \tag{6.6}$$

with $q_j = \{\sigma, \beta, \delta\psi, \delta\psi^*\}$ being the generalized coordinates.

First, the equations for $\sigma\left(t\right)$ and $\beta\left(t\right)$ are

$$\frac{\hbar^2}{2m_I\sigma^3} - \frac{2\hbar^2\beta^2\sigma}{m_I} - \hbar\dot{\beta}\sigma = \frac{g_{BI}\sqrt{\rho}}{\sqrt{\pi}} \int \left(\delta\psi + \delta\psi^*\right) \frac{2x^2 - \sigma^2}{\sigma^4} e^{-\frac{x^2}{\sigma^2}} \mathrm{d}x, \tag{6.7}$$

and

$$\beta = \frac{m_I}{2\hbar}\frac{\dot{\sigma}}{\sigma}. \tag{6.8}$$

By eliminating β, we obtain

$$\frac{d^2\sigma}{dt^2} = \frac{\hbar^2}{m_I^2\sigma^3} - \frac{2g_{BI}\sqrt{\rho}}{m_I\sqrt{\pi}\sigma^4} \int \left(\delta\psi + \delta\psi^*\right)\left(2x^2 - \sigma^2\right) e^{-\frac{x^2}{\sigma^2}} \mathrm{d}x. \tag{6.9}$$

Therefore the equation of motion of the width of the impurity is coupled to the condensate distortion.

For the distortion of the condensate, we have

$$\begin{aligned} i\hbar\frac{\partial}{\partial t}\delta\psi &= \left[-\frac{\hbar^2}{2m_B}\frac{\partial^2}{\partial x^2} + g_{BB}\rho\right]\delta\psi + g_{BB}\rho\delta\psi^* + \frac{g_{BI}\sqrt{\rho}}{\sqrt{\pi}\sigma}e^{-\frac{x^2}{\sigma^2}}, \\ -i\hbar\frac{\partial}{\partial t}\delta\psi^* &= \left[-\frac{\hbar^2}{2m_B}\frac{\partial^2}{\partial x^2} + g_{BB}\rho\right]\delta\psi^* + g_{BB}\rho\delta\psi + \frac{g_{BI}\sqrt{\rho}}{\sqrt{\pi}\sigma}e^{-\frac{x^2}{\sigma^2}}. \end{aligned} \tag{6.10}$$

To decouple $\delta\psi(x,t)$ and $\delta\psi^*(x,t)$, we write $\delta\psi(x,t)$ as

$$\delta\psi(x,t)=\sum_{k\neq 0}\left[Z_k(t)\,u_k\frac{e^{ikx}}{\sqrt{l}}-Z_k^*(t)\,v_k\frac{e^{-ikx}}{\sqrt{l}}\right], \tag{6.11}$$

where u_k and v_k were defined in (2.51). Here, l is the length of the system and $Z_k(t)$ are the time-dependent coherent amplitudes for the Bogoliubov excitations. Also, it is noticed that:

$$\frac{g_{BI}\sqrt{\rho}}{\sqrt{\pi}\sigma}e^{-\frac{x^2}{\sigma^2}}=\frac{g_{BI}\sqrt{\rho}}{2\pi}\int_{-\infty}^{\infty}e^{-\frac{k^2\sigma^2}{4}}e^{ikx}\mathrm{d}k=\sum_{k\neq 0}\frac{g_{BI}\sqrt{\rho}}{l}e^{-\frac{k^2\sigma^2}{4}}e^{ikx}. \tag{6.12}$$

Substituting (6.11) and (6.12) into (6.10), we have

$$\begin{aligned}
i\hbar\dot{Z}_k u_k&=\left(\frac{\hbar^2k^2}{2m_B}+g_{BB}\rho\right)u_kZ_k-g_{BB}\rho v_kZ_k+\frac{g_{BI}\sqrt{N}}{l}e^{-\frac{k^2\sigma^2}{4}},\\
i\hbar\dot{Z}_k v_k&=-\left(\frac{\hbar^2k^2}{2m_B}+g_{BB}\rho\right)v_kZ_k+g_{BB}\rho Z_ku_k.
\end{aligned} \tag{6.13}$$

After simplification, we obtain the equation for $Z_k(t)$:

$$i\hbar\dot{Z}_k=\xi(k)\,Z_k+\frac{g_{BI}\sqrt{N}}{l}\sqrt{\frac{\epsilon(k)}{\xi(k)}}e^{-\frac{k^2\sigma^2}{4}}. \tag{6.14}$$

Analytically, the formal solution for (6.14) is given by

$$Z_k(t)=Z_k(0)\,e^{-i\omega_k t}-\frac{i}{\hbar}\frac{g_{BI}\sqrt{N}}{l}\sqrt{\frac{\epsilon(k)}{\xi(k)}}\int_0^t e^{\frac{-k^2\sigma^2(t')}{4}}e^{-i\omega_k(t-t')}\mathrm{d}t'. \tag{6.15}$$

Here, we have introduced $\omega_k=\xi(k)/\hbar$ for notational convenience.

By (6.15), (6.11) becomes

$$\begin{aligned}
\delta\psi(x,t)=&\sum_{k\neq 0}\left[Z_k(0)\,u_k\frac{e^{i(kx-\omega_k t)}}{\sqrt{l}}-Z_k^*(0)\,v_k\frac{e^{-i(kx-\omega_k t)}}{\sqrt{l}}\right]\\
&-\frac{i}{\hbar}\sum_{k\neq 0}\frac{g_{BI}\sqrt{N}}{l\sqrt{l}}\sqrt{\frac{\epsilon(k)}{\xi(k)}}u_k\int_0^t e^{-\frac{k^2\sigma^2(t')}{4}}e^{i[kx-\omega_k(t-t')]}\mathrm{d}t'\\
&-\frac{i}{\hbar}\sum_{k\neq 0}\frac{g_{BI}\sqrt{N}}{l\sqrt{l}}\sqrt{\frac{\epsilon(k)}{\xi(k)}}v_k\int_0^t e^{-\frac{k^2\sigma^2(t')}{4}}e^{-i[kx-\omega_k(t-t')]}\mathrm{d}t'.
\end{aligned} \tag{6.16}$$

Using (6.16) and integrating with respect to x, the equation for $\sigma(x,t)$ becomes

$$\begin{aligned}\ddot{\sigma}(t) =& \frac{\hbar^2}{m_I^2\sigma^3(t)} \\ &+ \frac{g_{BI}\sqrt{\rho}\sigma(t)}{m_I\sqrt{l}}\sum_{k\neq 0}\sqrt{\frac{\epsilon(k)}{\xi(k)}}k^2 e^{-\frac{k^2\sigma^2(t)}{4}}\left[Z_k(0)\,e^{-i\omega_k t}+Z_k^*(0)\,e^{i\omega_k t}\right] \\ &- \frac{2g_{BI}^2\rho\sigma(t)}{\hbar m_I l}\sum_{k\neq 0}\frac{\epsilon(k)}{\xi(k)}k^2 e^{-\frac{k^2\sigma^2(t)}{4}}\int_0^t e^{-\frac{k^2\sigma^2(t')}{4}}\sin\left[\omega_k(t-t')\right]\mathrm{d}t'.\end{aligned} \tag{6.17}$$

To understand the equation more physically, we integrate the last term of (6.17) by parts. Furthermore, we are interested in the thermodynamical limit with $N\to\infty$ and $l\to\infty$, but keeping ρ fixed. In this case, the allowed values for k are nearly continuous, so we have replaced $\sum_k$ by $\frac{l}{2\pi}\int_\infty^\infty \mathrm{d}k$. Finally, we obtain the effective generalized Langevin equation [68] for $\sigma(t)$:

$$m_I\ddot{\sigma}(t) = F(\sigma) + \int_0^t K(t,t')\,\dot{\sigma}(t')\,\mathrm{d}t' + \eta(t) + \varsigma(t). \tag{6.18}$$

Here, the effective force is

$$\begin{aligned}F(\sigma) =& \frac{\hbar^2}{m_I\sigma^3(t)} - 2\sqrt{\frac{2}{\pi}}\frac{g_{BI}^2\rho m_B}{\hbar^2} \\ &+ \frac{4g_{BI}^2\rho m_B}{\hbar^3\sqrt{g_{BB}\rho m_B}}\sigma(t)\,\mathrm{Exp}\left[\frac{2g_{BB}\rho m_B}{\hbar^2}\sigma^2(t)\right]\mathrm{Erfc}\left[\frac{\sqrt{2g_{BB}\rho m_B}}{\hbar}\sigma(t)\right].\end{aligned} \tag{6.19}$$

The memory friction kernel is

$$K(t,t') = -\frac{g_{BI}^2\rho}{2\pi}\int_{-\infty}^{\infty}\left[\frac{\epsilon(k)}{\xi^2(k)}k^4\sigma(t)\,\sigma(t')\,e^{-\frac{k^2\sigma^2(t)}{4}}e^{-\frac{k^2\sigma^2(t')}{4}}\cos\omega_k(t-t')\right]\mathrm{d}k. \tag{6.20}$$

The noise term is

$$\eta(t) = \frac{g_{BI}\sqrt{N}\sigma(t)}{\pi}\int_{-\infty}^{\infty}\left[\sqrt{\frac{\epsilon(k)}{\xi(k)}}k^2 e^{-\frac{k^2\sigma^2(t)}{4}}Z_k(0)\cos\omega_k t\right]\mathrm{d}k. \tag{6.21}$$

Finally, the initial slip is given by

$$\varsigma(t) = \frac{g_{BI}^2\rho\sigma(t)}{\pi}\int_{-\infty}^{\infty}\left[\frac{\epsilon(k)}{\xi^2(k)}k^2 e^{-\frac{k^2\sigma^2(0)}{4}}e^{-\frac{k^2\sigma^2(t)}{4}}\cos\omega_k t\right]\mathrm{d}k. \tag{6.22}$$

From (6.19), we know that the equilibrium width σ_∞ satisfies the transcendental equation:

$$\begin{aligned}\frac{\hbar^2}{m_I\sigma_\infty^3} =& 2\sqrt{\frac{2}{\pi}}\frac{g_{BI}^2\rho m_B}{\hbar^2} \\ &- \frac{4g_{BI}^2\rho m_B}{\hbar^3\sqrt{g_{BB}\rho m_B}}\sigma_\infty \mathrm{Exp}\left[\frac{2g_{BB}\rho m_B}{\hbar^2}\sigma_\infty^2\right]\mathrm{Erfc}\left[\frac{\sqrt{2g_{BB}\rho m_B}}{\hbar}\sigma_\infty\right],\end{aligned} \tag{6.23}$$

which is the same as (5.22) after rescaling the variables according to (5.16). In addition, we obtain the effective potential for the system by integrating (6.19) with respect to σ:

$$V(\sigma) = \frac{\hbar^2}{2m_I\sigma^2} - \frac{g_{BI}^2\rho}{\hbar}\sqrt{\frac{m_B}{g_{BB}\rho}}\mathrm{Exp}\left[\frac{2g_{BB}m_B\rho}{\hbar^2}\sigma^2\right]\mathrm{Erfc}\left(\frac{\sqrt{2g_{BB}m_B\rho}}{\hbar}\sigma\right). \tag{6.24}$$

6.2 Small amplitude oscillation

6.2.1 Period and damping rate

The nonlinear potential in (6.24) can be approximated as harmonic:

$$V(\sigma) \approx V(\sigma_\infty) + \frac{1}{2}\left.\frac{d^2V}{d\sigma^2}\right|_{\sigma_\infty}(\sigma-\sigma_\infty)^2. \tag{6.25}$$

Since the potential is bounded, the evolution of $\sigma(t)$ is periodic. By defining the effective spring constant as

$$\kappa = \left.\frac{d^2V}{d\sigma^2}\right|_{\sigma_\infty}, \tag{6.26}$$

the period of the oscillation is approximately given by

$$T = 2\pi\sqrt{\frac{m_I}{\kappa}}. \tag{6.27}$$

Furthermore, the interaction between the impurity atom and the condensate atoms induces dissipation, so the amplitude of oscillation for $\sigma(t)$ should decay.

In the following, we obtain an approximated model to describe the dynamics for the system.

Since $\sigma(t) \approx \sigma_\infty$, we write it as

$$\sigma(t) = \sigma_\infty + \varepsilon(t), \tag{6.28}$$

with $\varepsilon(t)$ responsible for the oscillation. As $\varepsilon(t)/\sigma_\infty \ll 1$, we linearize the equation by expanding (6.18) up to first order in $\varepsilon(t)$. Then, the equation for $\varepsilon(t)$ is given by

$$\begin{aligned}\ddot{\varepsilon}(t) =& -\Omega^2\varepsilon(t) \\ &- \int_0^t \left[\int_{-\infty}^{\infty} \frac{g_{BI}^2\rho}{2\pi m_I}\frac{\epsilon(k)}{\xi^2(k)}k^4\sigma_\infty^2 e^{-\frac{k^2\sigma_\infty^2}{2}}\cos\omega_k(t-t')\mathrm{d}k\right]\dot{\varepsilon}(t')\,\mathrm{d}t',\end{aligned} \tag{6.29}$$

where Ω is the natural angular frequency of the oscillation under the harmonic approximation. Here, the term for the initial slip has been neglected. Also, we consider the system, in which the interaction between the impurity atom and the condensate is set to zero initially, so $Z_k(0) = 0$ and the noise term has been dropped.

When the damping rate is small, so that the change in the amplitude of $\varepsilon(t)$ within the interval t' to t is negligible, we have

$$\varepsilon(t') \approx \varepsilon(t)\cos\Omega(t-t') - \frac{\dot{\varepsilon}(t)}{\Omega}\sin\Omega(t-t'). \tag{6.30}$$

Using (6.30), the nonlinear damping term in (6.29) becomes

$$\begin{aligned}&-\Omega\varepsilon(t)\int_0^t\int_{-\infty}^{\infty}\frac{g_{BI}^2\rho\sigma_\infty^2}{2\pi m_I}\frac{\epsilon(k)}{\xi^2(k)}k^4 e^{-\frac{k^2\sigma_\infty^2}{2}}\cos\omega_k(t-t')\sin\Omega(t-t')\mathrm{d}k\mathrm{d}t' \\ &-\dot{\varepsilon}(t)\int_0^t\int_{-\infty}^{\infty}\frac{g_{BI}^2\rho\sigma_\infty^2}{2\pi m_I}\frac{\epsilon(k)}{\xi^2(k)}k^4 e^{-\frac{k^2\sigma_\infty^2}{2}}\cos\omega_k(t-t')\cos\Omega(t-t')\mathrm{d}k\mathrm{d}t'.\end{aligned} \tag{6.31}$$

Integrating with respect to t, we obtain

$$\begin{aligned}&-\Omega\varepsilon(t)\frac{g_{BI}^2\rho\sigma_\infty^2}{2\pi m_I}\int_{-\infty}^{\infty}\frac{\epsilon(k)}{\xi^2(k)}k^4 e^{-\frac{k^2\sigma_\infty^2}{2}}\left[\frac{\Omega}{\Omega^2-\omega_k^2} - \frac{\cos(\Omega-\omega_k)t}{2(\Omega-\omega_k)} - \frac{\cos(\Omega+\omega_k)t}{2(\Omega+\omega_k)}\right]\mathrm{d}k \\ &-\dot{\varepsilon}(t)\frac{g_{BI}^2\rho\sigma_\infty^2}{4\pi m_I}\int_{-\infty}^{\infty}\frac{\epsilon(k)}{\xi^2(k)}k^4 e^{-\frac{k^2\sigma_\infty^2}{2}}\left[\frac{\sin(\Omega+\omega_k)t}{\Omega+\omega_k} + \frac{\sin(\Omega-\omega_k)t}{\Omega-\omega_k}\right]\mathrm{d}k.\end{aligned} \tag{6.32}$$

The first term corresponds to the shift in the period of oscillation, whereas the second term corresponds to the damping of $\sigma(t)$. Furthermore, it is noticed that the damping is mainly contributed from the creation of phonons with energy $\xi(k) = \xi(k_\Omega)$, where k_Ω and Ω are related to each other through the Bogoliubov dispersion. When $(\Omega - \omega_k)\, t \gg 1$, the counter rotating terms can be neglected, so the equation for $\varepsilon(t)$ reduces to

$$\begin{aligned}\ddot{\varepsilon}(t) = &-\Omega^2 \varepsilon(t) \\ &- \Omega\varepsilon(t)\, \frac{g_{BI}^2 \rho \sigma_\infty^2}{2\pi m_I} \int_{-\infty}^{\infty} \frac{\epsilon(k)}{\xi^2(k)} k^4 e^{-\frac{k^2\sigma_\infty^2}{2}} \left[\frac{\Omega}{\Omega^2 - \omega_k^2} - \frac{\cos(\Omega - \omega_k)\, t}{2(\Omega - \omega_k)}\right] \mathrm{d}k \\ &- \dot{\varepsilon}(t)\, \frac{g_{BI}^2 \rho \sigma_\infty^2}{4\pi m_I} \int_{-\infty}^{\infty} \frac{\epsilon(k)}{\xi^2(k)} k^4 e^{-\frac{k^2\sigma_\infty^2}{2}} t\mathrm{sinc}\left[(\Omega - \omega_k)\, t\right] \mathrm{d}k. \end{aligned} \tag{6.33}$$

If we focus on the damping rate, we need to evaluate the following integral:

$$\Gamma = \frac{g_{BI}^2 \rho \sigma_\infty^2}{4\pi m_I} \int_{-\infty}^{\infty} \frac{\epsilon(k)}{\xi^2(k)} k^4 e^{-\frac{k^2\sigma_\infty^2}{2}} t\mathrm{sinc}\left[(\Omega - \omega_k)\, t\right] \mathrm{d}k. \tag{6.34}$$

When $(\Omega - \omega_k)\, t \gg 1$, we have

$$t\mathrm{sinc}\left[(\Omega - \omega_k)\, t\right] \approx \delta(\Omega - \omega_k), \tag{6.35}$$

so Γ can be approximated as

$$\Gamma = \frac{g_{BI}^2 \rho \sigma_\infty^2}{4\pi m_I} \int_{-\infty}^{\infty} \frac{\epsilon(k)}{\xi^2(k)} k^4 e^{-\frac{k^2\sigma_\infty^2}{2}} \delta(\Omega - \omega_k)\, \mathrm{d}k. \tag{6.36}$$

From (6.33) and (6.36), the dynamics for the slowly-damping system can be approximated by the equation:

$$\ddot{\varepsilon}(t) + \Gamma\dot{\varepsilon}(t) + \left(\Omega^2 + \Delta^2\right)\varepsilon(t) = 0, \tag{6.37}$$

where Δ is the shift in the angular frequency given by

$$\Delta = \sqrt{\frac{g_{BI}^2 \rho \sigma_\infty^2 \Omega}{2\pi m_I} \int_{-\infty}^{\infty} \frac{\epsilon(k)}{\xi^2(k)} k^4 e^{-\frac{k^2\sigma_\infty^2}{2}} \left[\frac{\Omega}{\Omega^2 - \omega_k^2} - \frac{\cos(\Omega - \omega_k)\, t}{2(\Omega - \omega_k)}\right] \mathrm{d}k}. \tag{6.38}$$

Clearly, (6.37) admits the solution:

$$\varepsilon(t) = A e^{-\frac{\Gamma t}{2}} \cos\left[\left(\Omega^2 + \Delta^2 - \frac{\Gamma^2}{4}\right) t + \theta\right], \tag{6.39}$$

where θ is the phase angle depending on the initial conditions.

6.2.2 Numerical test

To check the validity of (6.39), we consider a system consisting of a ^{85}Rb impurity atom immersed in ^{23}Na condensate with $\rho = 10^8$. The atoms are trapped harmonically in the transverse directions with $\omega_\perp = 2\pi \times 500$ Hz. Due to the tight confinement in the transverse directions, the system can be approximated as one-dimensional. The scattering length between the condensate atoms is set to 3 nm. Initially, the impurity atom and the condensate is non-interacting. We suddenly increase the scattering length between the impurity atom and the condensate atom to 42 nm at $t = 0$, which gives $g_{BI}/g_{BB} = 14$. Under this configuration, $Z_k(0) = 0$ and the noise term can be dropped. In addition, $\zeta \approx 6$ with $\sigma_\infty \approx 0.788$ (in unit of χ). To achieve small amplitude oscillation, we set $\sigma_0 = 0.8$. We plot the exact potential and the corresponding approximated harmonic potential for this configuration in Fig. 6.1.

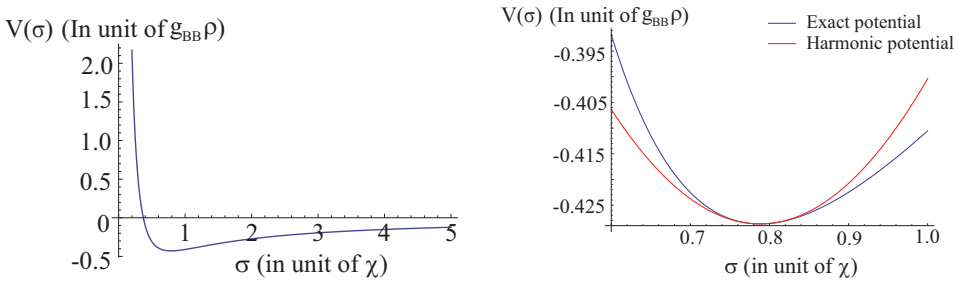

Figure 6.1: The effective potential for the system (left) and the comparison with its approximated harmonic potential near σ_∞ (right).

We numerically solve (6.18) to obtain $\sigma(t)$ from $t = 0$ to $t = 1000$ and plot the results in Fig. 6.2. Also, we compare the numerical result with the approximated model at $t = 800$ to $t = 1000$ and plot them in Fig. 6.3. From the figure, we see that the result from the approximated model agrees with the numerical result well.

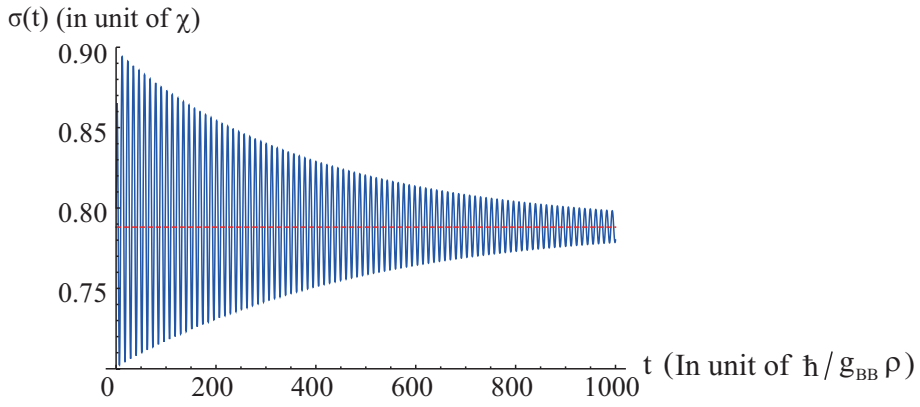

Figure 6.2: The numerical result for $\sigma(t)$ (blue solid line) and the equilibrium width (red dashed line).

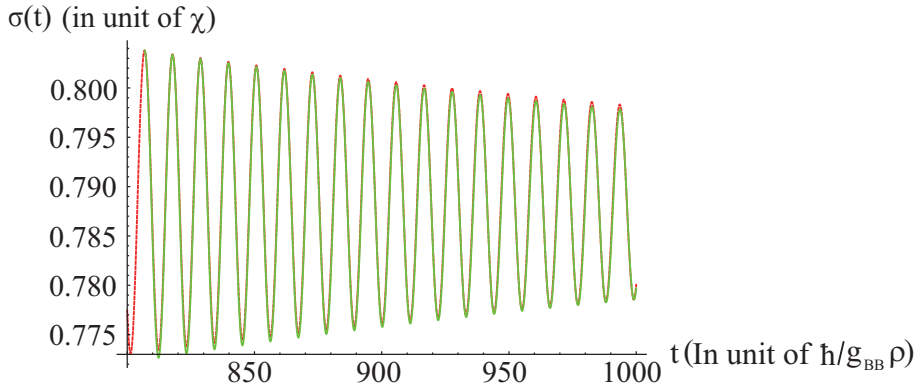

Figure 6.3: Comparison between the numerical result (red line) and the approximated model (green line).

6.3 Large amplitude oscillation

Apart from the small amplitude oscillation, it is interesting to consider the nonlinear effects for the system when $\sigma(t)$ has large amplitude of oscillation. For this case, we need to solve (6.18) numerically. For better comparison, we consider the same system as the previous section. However, we set $\sigma_0 = 5$ to achieve large amplitude oscillation.

The effective potential in (6.24) is bounded, so we expect that $\sigma(t)$ undergoes periodic motion, with the period given by

$$T = \sqrt{2m_I}\left|\int_{\sigma_0}^{\sigma_1} \frac{\mathrm{d}\sigma}{\sqrt{V(\sigma_0) - V(\sigma)}}\right|. \tag{6.40}$$

Here, σ_1 satisfies $V(\sigma_1) = V(\sigma_0)$. For the present case, we have $T \approx 65$, in unit of $\hbar/(g_{BB}\rho)$, which provides a rough approximation to the numerical result shown in Fig. 6.4. The difference between the approximated period and the numerical result comes from the nonlinear damping.

In addition, the slope of the nonlinear potential is large when $\sigma < 0.6$, so a slight change in σ leads to a dramatic change in the potential. This hard core repulsion results in the cusp-like minimums for $\sigma(t)$. It is interesting that the cusp-like features resemble the bubble dynamics in sonoluminescene [69]. When $\sigma(t)$ reaches the minimums, the energy of the impurity atom increases as larger quantum pressure exerts on it. It is expected that the energy stored should release and propagate away from the impurity atom through phonon pulses when $\sigma(t)$ increases from the minimums.

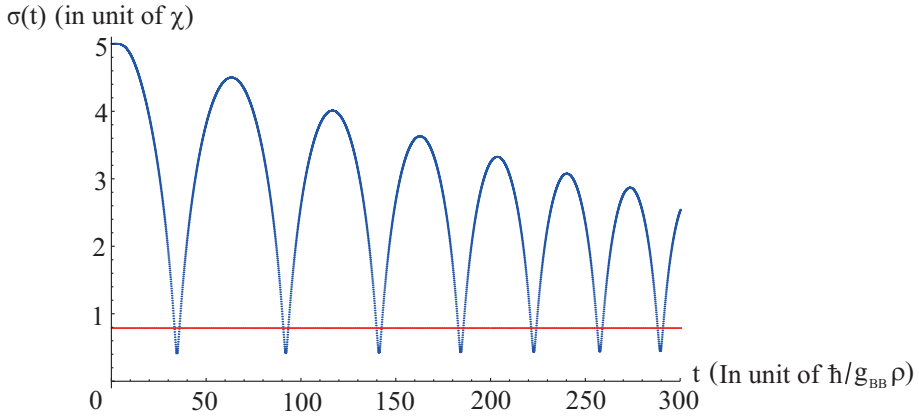

Figure 6.4: Time evolution for $\sigma(t)$ with the initial condition $\sigma_0 = 5$ is chosen. The blue line represents the result from numerical simulation and the red dashed line represents the equilibrium width σ_∞.

For illustration, we have numerically simulated the condensate wave function by using the result of $\sigma(t)$ and (6.10) at the time near the first minimum for $\sigma(t)$. The probability amplitudes for the condensate wave functions $|\psi(x,t)|^2$ at different times are plotted in Fig. 6.5. From the figure, it is observed that the phonon pulse is formed when $\sigma(t)$ increases from the minimum position, which indicates the release of the energy stored in the impurity atom.

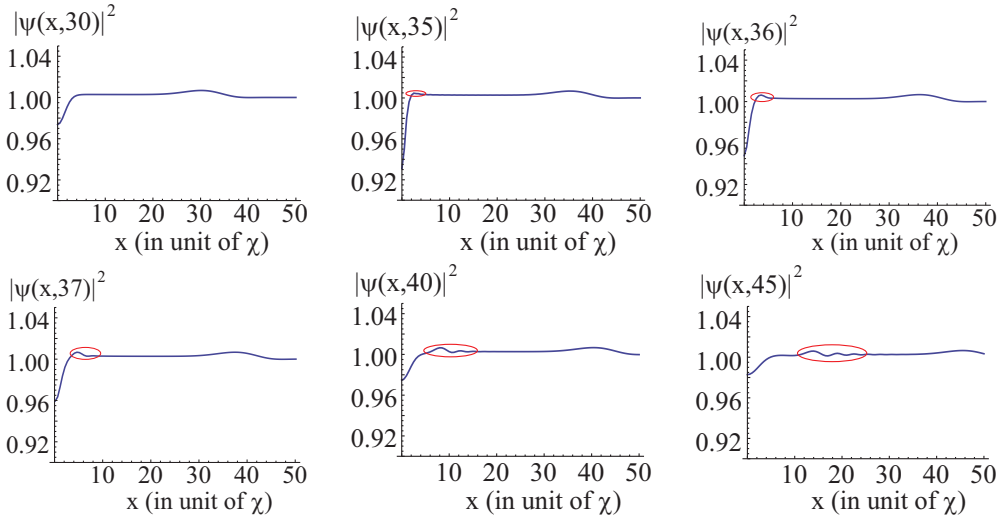

Figure 6.5: Snapshots of the probability amplitude for the condensate wave function $|\psi(x,t)|^2$ at $t = 30$, $t = 35$, $t = 36$, $t = 37$, $t = 40$ and $t = 45$. It is reminded that $\sigma(t)$ attends its first minimum at $t \approx 34$. The red circles indicate the formation of the phonon pulse.

Chapter 7

Conclusions

In this thesis, we have studied various one-dimensional systems with interacting ultracold atoms. In the first part of the thesis, we considered the system with two or three interacting atoms. Different from most previous studies of the same system, we provided an analysis of the quantum correlation of the system through the Schmidt decomposition. We concluded that about three to four Schmidt modes are required to describe the ground state of the system when $0 \leq g \leq 15$. In addition, we have evaluated the second order coherence function and successfully obtained analytic results for a Tonks gas with two to five atoms. For the three-atom system, we proposed the finite difference method to diagonalize the Hamiltonian. Since the method does not based on the expansion in basis functions, it can be applied to strongly interacting systems effectively.

In the second part of the thesis, we have studied the system with an impurity atom. In the case where the background is a harmonically trapped Tonks gas, we constructed the wave function of the system using the generalized Bose-Fermi mapping theorem. To address the spatial distribution of the impurity atom, we evaluated its single particle density numerically and discovered that the results can be well fitted by Gaussian distributions if the impurity atom is placed at the middle of the system. Also, we have considered the situation

when the impurity atom is placed at one side of the system and discussed the differences due to the change in the configuration.

When the background is a Bose-Einstein condensate, we applied the Bogoliubov approximation and the variational principle, and observed that the impurity atom can become self-localized with a width, depending on the trapping parameter only. Guided by the particular solution in [57], we identified that the ground state wave function for the impurity atom can be better approximated by the hyperbolic secant trial wave function. We found that the energy is about 2% lower as compared with the traditional Gaussian trial wave function. In addition, we have successfully obtained an approximated formula for the coherent amplitudes in the small-k regime by considering the Fröhlich polaron Hamiltonian of the system.

Lastly, we focused on the dynamics of the impurity atom. To obtain the width of the impurity wave function as a function of time, we applied the time-dependent variational principle and derived the effective generalized Langevin equation. By solving the equation, we obtained good approximations to the period of oscillation and the damping rate for the width, when its amplitude of oscillation is small. When the width has a large amplitude of oscillation, we solved the Langevin equation numerically and observed the emission of phonon pulses during the oscillation.

Bibliography

[1] S. Bose, Z. Physik. **26**, 178 (1924).

[2] A. Einstein, Sitzber. Kgl. Preuss. Akad.Wiss. (1924).

[3] A. Einstein, Sitzber. Kgl. Preuss. Akad.Wiss. (1925).

[4] M. H. Anderson, J. R. Ensher, M. R. Matthews, C. E. Wieman, and E. A. Cornell, Science **269**, 198 (1995).

[5] C. Bradley, C. Sackett, J. Tollett, and R. Hulet, Phys. Rev. Lett. **75**, 1687 (1995).

[6] K. Davis, M.-O. Mewes, M. v. Andrews, N. Van Druten, D. Durfee, D. Kurn, and W. Ketterle, Phys. Rev. Lett. **75**, 3969 (1995).

[7] K. S. Novoselov, Z. Jiang, Y. Zhang, S. Morozov, H. Stormer, U. Zeitler, J. Maan, G. Boebinger, P. Kim, and A. Geim, Science **315**, 1379 (2007).

[8] H. L. Stormer, Rev. Mod. Phys. **71**, 875 (1999).

[9] X.-L. Qi and S.-C. Zhang, Rev. Mod. Phys. **83**, 1057 (2011).

[10] M. Girardeau, J. Math. Phys. **1**, 516 (1960).

[11] M. Girardeau, Phys. Rev. B **139** (1965).

[12] J. Esteve, J.-B. Trebbia, T. Schumm, A. Aspect, C. I. Westbrook, and I. Bouchoule, Phys. Rev. Lett. **96**, 130403 (2006).

[13] A. Görlitz, J. M. Vogels, A. E. Leanhardt, C. Raman, T. L. Gustavson, J. R. Abo-Shaeer, A. P. Chikkatur, S. Gupta, S. Inouye, T. Rosenband, and W. Ketterle, Phys. Rev. Lett. **87**, 130402 (2001).

[14] M. Greiner, I. Bloch, O. Mandel, T. W. Hänsch, and T. Esslinger, Phys. Rev. Lett. **87**, 160405 (2001).

[15] H. Moritz, T. Stöferle, M. Köhl, and T. Esslinger, Phys. Rev. Lett. **91**, 250402 (2003).

[16] F. Schreck, L. Khaykovich, K. L. Corwin, G. Ferrari, T. Bourdel, J. Cubizolles, and C. Salomon, Phys. Rev. Lett. **87**, 080403 (2001).

[17] T. Stöferle, H. Moritz, C. Schori, M. Köhl, and T. Esslinger, Phys. Rev. Lett. **92**, 130403 (2004).

[18] T. Fukuhara, A. Kantian, M. Endres, M. Cheneau, P. Schauß, S. Hild, D. Bellem, U. Schollwöck, T. Giamarchi, C. Gross, I. Bloch, and S. Kuhr, Nat Phys **9** (2013).

[19] M. A. Cazalilla, R. Citro, T. Giamarchi, E. Orignac, and M. Rigol, Rev. Mod. Phys. **83**, 1405 (2011).

[20] K. Huang, *Statistical Mechanics*, Wiley, New York, 1987.

[21] M. Olshanii, Phys. Rev. Lett. **81**, 938 (1998).

[22] E. H. Lieb, Phys. Rev. **130**, 1616 (1963).

[23] E. H. Lieb and W. Liniger, Phys. Rev. **130**, 1605 (1963).

[24] C. Chin, R. Grimm, P. Julienne, and E. Tiesinga, Rev. Mod. Phys. **82**, 1225 (2010).

[25] H. Feshbach, Ann. Phys. **18**, 287 (1962).

[26] S. Inouye, M. Andrews, J. Stenger, H.-J. Miesner, D. Stamper-Kurn, and W. Ketterle, Nature **392**, 151 (1998).

[27] E. Timmermans, P. Tommasini, M. Hussein, and A. Kerman, Physics Reports **315**, 199 (1999).

[28] M. Girardeau and E. Wright, Laser Physics **12**, 8 (2002).

[29] M. D. Girardeau and E. M. Wright, Phys. Rev. Lett. **84**, 5239 (2000).

[30] M. D. Girardeau, E. M. Wright, and J. M. Triscari, Phys. Rev. A **63**, 033601 (2001).

[31] J. Goold and T. Busch, Phys. Rev. A **77**, 063601 (2008).

[32] R. Pezer and H. Buljan, Phys. Rev. Lett. **98**, 240403 (2007).

[33] B.-B. Wei, S.-J. Gu, and H.-Q. Lin, Phys. Rev. A **79**, 063627 (2009).

[34] T. Kinoshita, T. Wenger, and D. S. Weiss, Science **305**, 1125 (2004).

[35] B. Paredes, A. Widera, V. Murg, O. Mandel, S. Fölling, I. Cirac, G. V. Shlyapnikov, T. W. Hänsch, and I. Bloch, Nature **429**, 277 (2004).

[36] S. Palzer, C. Zipkes, C. Sias, and M. Köhl, Phys. Rev. Lett. **103**, 150601 (2009).

[37] C. J. Pethick and H. Smith, *Bose-Einstein condensation in dilute gases*, Cambridge university press, 2002.

[38] X. He, P. Xu, J. Wang, and M. Zhan, Opt Express **18**, 13586 (2010).

[39] Y. Miroshnychenko, W. Alt, I. Dotsenko, L. Förster, M. Khudaverdyan, D. Meschede, S. Reick, and A. Rauschenbeutel, Phys. Rev. Lett. **97**, 243003 (2006).

[40] I. Brouzos and P. Schmelcher, Phys. Rev. Lett. **108**, 045301 (2012).

[41] B. Chatterjee, I. Brouzos, S. Zöllner, and P. Schmelcher, Phys. Rev. A **82**, 043619 (2010).

[42] S. Zöllner, H.-D. Meyer, and P. Schmelcher, Phys. Rev. A **74**, 063611 (2006).

[43] S. Zöllner, H.-D. Meyer, and P. Schmelcher, Phys. Rev. A **75**, 043608 (2007).

[44] S. Zöllner, H.-D. Meyer, and P. Schmelcher, Phys. Rev. Lett. **100**, 040401 (2008).

[45] K. R. Thomas Busch, Berthold-Georg Englert and M. Wilkens, Foundations of Physics **28** (1998).

[46] M. Abramowitz and I. A. Stegun, *Handbook of Mathematical Functions*, Dover, New York, 1972.

[47] A. Ekert and P. L. Knight, American Journal of Physics **63**, 415 (1995).

[48] Y. Shi, Phys. Rev. A **67**, 024301 (2003).

[49] M. C. Tichy, F. de Melo, M. Kuś, F. Mintert, and A. Buchleitner, Fortschritte der Physik (2012).

[50] F. Deuretzbacher, K. Bongs, K. Sengstock, and D. Pfannkuche, Phys. Rev. A **75**, 013614 (2007).

[51] G. Astrakharchik, D. Blume, S. Giorgini, and B. Granger, Journal of Physics B: Atomic, Molecular and Optical Physics **37**, S205 (2004).

[52] S. Zöllner, H.-D. Meyer, and P. Schmelcher, Phys. Rev. A **78**, 013621 (2008).

[53] R. Kosloff and H. Tal-Ezer, Chem. Phys. Lett. **127**, 223 (1986).

[54] M. D. Girardeau and A. Minguzzi, Phys. Rev. Lett. **99**, 230402 (2007).

[55] A. P. Chikkatur, A. Görlitz, D. M. Stamper-Kurn, S. Inouye, S. Gupta, and W. Ketterle, Phys. Rev. Lett. **85**, 483 (2000).

[56] F. M. Cucchietti and E. Timmermans, Phys. Rev. Lett. **96**, 210401 (2006).

[57] K. Sacha and E. Timmermans, Phys. Rev. A **73**, 063604 (2006).

[58] M. Bruderer, W. Bao, and D. Jaksch, EPL **82**, 30004 (2008).

[59] W. Casteels, T. Cauteren, J. Tempere, and J. Devreese, Laser Physics **21**, 1480 (2011).

[60] W. Casteels, J. Tempere, and J. Devreese, Phys. Rev. A **84**, 063612 (2011).

[61] D. Santamore and E. Timmermans, New Journal of Physics **13**, 103029 (2011).

[62] J. Tempere, W. Casteels, M. K. Oberthaler, S. Knoop, E. Timmermans, and J. T. Devreese, Phys. Rev. B **80**, 184504 (2009).

[63] J. Catani, G. Lamporesi, D. Naik, M. Gring, M. Inguscio, F. Minardi, A. Kantian, and T. Giamarchi, Phys. Rev. A **85**, 023623 (2012).

[64] T. H. Johnson, M. Bruderer, Y. Cai, S. R. Clark, W. Bao, and D. Jaksch, EPL **98**, 26001 (2012).

[65] S. Peotta, D. Rossini, M. Polini, F. Minardi, and R. Fazio, Phys. Rev. Lett. **110**, 015302 (2013).

[66] V. M. Pérez-García, H. Michinel, J. I. Cirac, M. Lewenstein, and P. Zoller, Phys. Rev. Lett. **77**, 5320 (1996).

[67] V. M. Pérez-García, H. Michinel, J. I. Cirac, M. Lewenstein, and P. Zoller, Phys. Rev. A **56**, 1424 (1997).

[68] U. Weiss, *Quantum Dissipative Systems*, World Scientific, fourth edition, 2012, See page 20-23.

[69] S. J. Putterman, Scientific American **272**, 46 (1995).

[70] R. Robinett, *Quantum Mechanics: Classical Results, Modern Systems, and Visualized Examples: Classical Results, Modern Systems, and Visualized Examples*, OUP Oxford, 2006, See subsection 15.3.3.

Appendix A

Numerical method for system of three interacting atoms

In chapter 3, we have numerically diagonalized the Hamiltonian for the system of three interacting atoms through finite difference method. In this appendix, we provide more details for the numerical approach. To make the discussion more effective, the original system has been rotated with angle $\pi/6$ in the clockwise direction.

A.1 Discretization for the Schrödinger's equation

Fig. A.1 shows the region where finite difference would be performed. The region would be discretized and the values of $\psi(X, Y)$ would be obtained on those dots, labelled as (X_i, Y_j). The horizontal and vertical separation between two neighbouring points are ΔX and ΔY respectively. Due to the geometry of the region, ΔY and ΔX are related by $\Delta Y = \sqrt{3}\Delta X$.

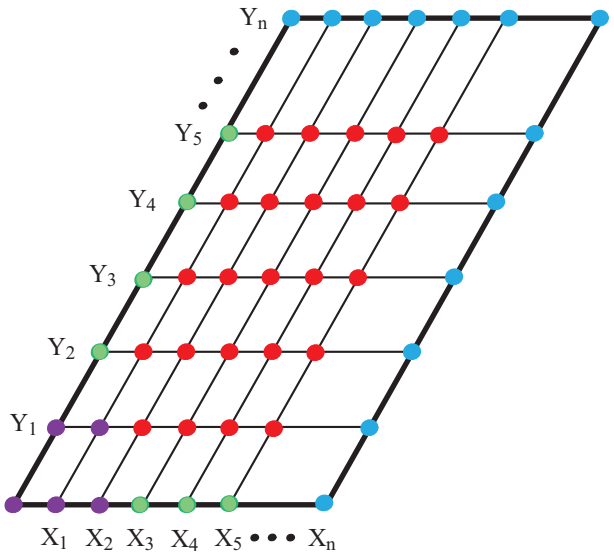

Figure A.1: The grids for finite difference method.

The discretized form of (A.2) is given by:

$$\begin{aligned} &-\frac{1}{2}\left[\frac{\psi\left(X_{i+1},Y_j\right)-2\psi\left(X_i,Y_j\right)+\psi\left(X_{i-1},Y_j\right)}{\left(\Delta X\right)^2}\right] \\ &-\frac{1}{2}\left[\frac{\psi\left(X_i,Y_{j+1}\right)-2\psi\left(X_i,Y_j\right)+\psi\left(X_i,Y_{j-1}\right)}{\left(\Delta Y\right)^2}\right] \\ &+\frac{1}{2}\left(X_i^2+Y_j^2\right)\psi\left(X_i,Y_j\right) \\ =&E_{X,Y}\psi\left(X_i,Y_j\right). \end{aligned} \tag{A.1}$$

where $X_i = i\Delta X$ and $Y_j = j\Delta Y$.

A.2 Boundary conditions

Inside the region bounded by the thick black lines, the time-independent Schrödinger equation is given by

$$\left[-\frac{1}{2}\left(\frac{\partial^2}{\partial X^2}+\frac{\partial^2}{\partial Y^2}\right)+\frac{1}{2}\left(X^2+Y^2\right)\right]\psi\left(X,Y\right)=E_{X,Y}\psi\left(X,Y\right). \tag{A.2}$$

The boundary condition at $Y = 0$ can be obtained by integrating (A.2):

$$\int_{Y=-\epsilon}^{Y=\epsilon} \left[-\frac{1}{2}\left(\frac{\partial^2}{\partial X^2} + \frac{\partial^2}{\partial Y^2} \right) + \frac{g}{\sqrt{2}}\delta\left(Y\right) + \frac{g}{\sqrt{2}}\delta\left(\frac{\sqrt{3}X - Y}{2} \right) \right]$$
$$= \int_{Y=-\epsilon}^{Y=\epsilon} E_{X,Y}\psi\left(X,Y\right) \mathrm{d}Y. \tag{A.3}$$

Using the continuity of wave function, (A.3) gives:

$$\frac{\partial}{\partial Y}\psi\left(X,Y\right)|_{Y=0^+} = \frac{g}{\sqrt{2}}\psi\left(X,0\right). \tag{A.4}$$

The boundary condition at $Y = \sqrt{3}X$ can be obtained with similar argument. Replacing $\left(\sqrt{3}X - Y\right)/2$ as R, the required boundary condition is given by:

$$\frac{\partial}{\partial Y}\psi|_{R=0^+} = \frac{g}{\sqrt{2}}\psi\left(R=0\right). \tag{A.5}$$

Therefore, the interaction has been turned into boundary conditions. To discretize the boundary condition in (A.4), ψ would be approximated by a degree two polynomial $j\left(Y\right)$ (X has been dropped for convenience), with the same values as ψ at the points T_1, T_2 and T_3 as illustrated in FIG. A.2. The aim is to relate $\psi\left(T_1\right)$ to $\psi\left(T_2\right)$ and $\psi\left(T_3\right)$.

Since j is a degree two polynomial in Y, we have:

$$j\left(Y\right) = AY^2 + BY + C \quad \text{and} \quad \frac{d}{dY}j\left(Y\right)|_{Y=0^+} = B. \tag{A.6}$$

Solving B in terms of ψ at T_1, T_2 and T_3, eq.(A.3) gives

$$\frac{g}{\sqrt{2}}\psi\left(T_1\right) = \frac{4\psi\left(T_2\right) - \psi\left(T_3\right) - 3\psi\left(T_1\right)}{2\Delta Y}. \tag{A.7}$$

Rearranging term, $\psi\left(T_1\right)$ is

$$\psi\left(T_1\right) = c_1\left[4\psi\left(T_2\right) - \psi\left(T_3\right)\right], \tag{A.8}$$

where c_1 is defined as

$$c_1 = \left(3 + \sqrt{6}g\Delta X\right)^{-1}. \tag{A.9}$$

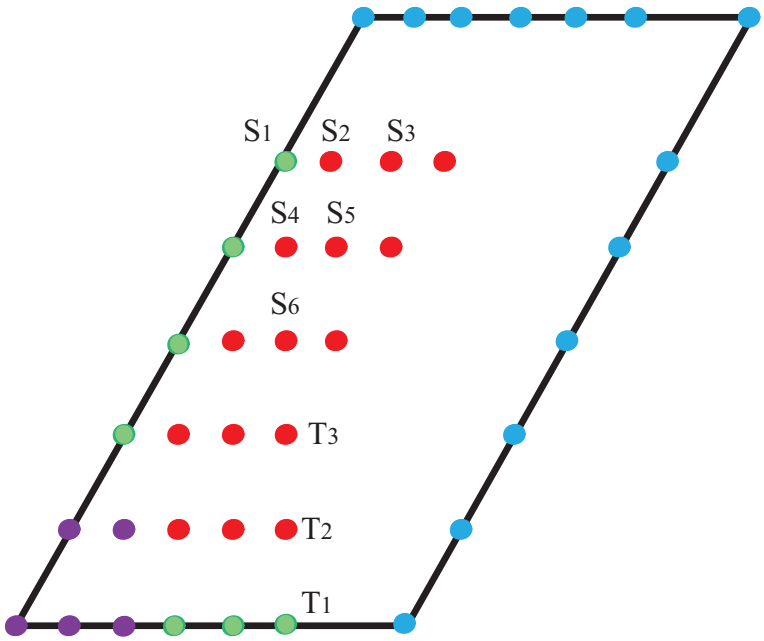

Figure A.2: Discretization for the boundary conditions.

For the boundary condition in (A.5), a degree two polynomial $k(X,Y)$ with the same values as ψ at the points S_1 - S_6 would be used:

$$k(X,Y) = aX^2 + bY^2 + cXY + dX + eY + f. \tag{A.10}$$

The aim is to relate $\psi(S_1)$ to $\psi(S_2)$, $\psi(S_3)$, $\psi(S_4)$, $\psi(S_5)$ and $\psi(S_6)$. After moving S_1 to the origin, the normal derivative at the inclined line is given by:

$$\frac{\partial}{\partial R}k(X,Y)\,|_{R=0^+} = \frac{\sqrt{3}}{2}d - \frac{1}{2}e. \tag{A.11}$$

Solving d and e in terms of the values of ψ at the points, (A.5) gives:

$$\begin{aligned}\frac{g}{\sqrt{2}}\psi(S_1) = &-\frac{\sqrt{3}}{2}\left[\frac{3\psi(S_1) - 4\psi(S_1) + \psi(S_3)}{2\Delta X}\right] \\ &-\frac{1}{2}\left[\frac{3\psi(S_1) - 4\psi(S_4) + \psi(S_6)}{2\Delta Y}\right].\end{aligned} \tag{A.12}$$

Rearranging terms, $\psi(S_1)$ would be given by

$$\psi(S_1) = c_2\left[4\psi(S_4) - \psi(S_6) + 12\psi(S_2) - 3\psi(S_3)\right], \tag{A.13}$$

where c_2 is defined as

$$c_2 = \left(12 + 2\sqrt{6}g\Delta X\right)^{-1}. \tag{A.14}$$

A.3 Some special points

Although (A.1), (A.8) and (A.13) give the necessary boundary conditions in terms of the values of ψ on the points, there are some special points, marked in purple color should be treated separately.

First, consider $\psi(X_2, Y_2)$ and $\psi(X_2, Y_0)$, it should be related to $\psi(X_3, Y_2)$, $\psi(X_4, Y_2)$, $\psi(X_2, Y_1)$ and $\psi(X_2, Y_0)$ due to (A.13). However, $\psi(X_2, Y_0)$ should be determined by $\psi(X_2, Y_1)$ and $\psi(X_2, Y_2)$ at the same time according to (A.8). Therefore, combining these two relationship gives:

$$\begin{aligned}&\psi(X_2, Y_2)\\ =&\frac{c_2}{1-c_1c_2}\left[4(1-c_1)\psi(X_2, Y_1)+12\psi(X_3, Y_2)-3\psi(X_4, Y_2)\right]\end{aligned} \tag{A.15}$$

and

$$\begin{aligned}&\psi(X_2, Y_0)\\ =&\frac{c_1}{1-c_1c_2}\left[4(1-c_2)\psi(X_2, Y_1)-12c_2\psi(X_3, Y_2)-3c_2\psi(X_4, Y_2)\right].\end{aligned} \tag{A.16}$$

For (X_1, Y_0) and (X_1, Y_1), it is necessary to sacrifice and approximate ψ by a linear function. Thus, the boundary condition for $Y = 0$ gives:

$$\frac{\psi(X_1, Y_1)-\psi(X_1, Y_0)}{\Delta Y}=\frac{g}{\sqrt{2}}\psi(X_1, Y_0). \tag{A.17}$$

Rearranging terms, $\psi(X_1, Y_0)$ is approximated by:

$$\psi(X_1, Y_0)=c_3\psi(X_1, Y_1), \tag{A.18}$$

where c_3 is defined as

$$c_3=\left(1+\sqrt{\frac{3}{2}}g\Delta X\right)^{-1}. \tag{A.19}$$

The boundary condition for the inclined line gives:

$$\begin{aligned}&\left[\frac{3\psi(X_1, Y_0)+\psi(X_2, Y_1)}{4}-\psi(X_1, Y_1)\right]\left(\frac{\sqrt{3}}{2}\Delta X\right)^{-1}\\ =&\frac{g}{\sqrt{2}}\psi(X_1, Y_1).\end{aligned} \tag{A.20}$$

Rearranging terms, $\psi(X_1, Y_1)$ is approximated by:

$$\psi(X_1, Y_1) = \frac{c_4}{4}\left[3\psi(X_1, Y_0) + \psi(X_2, Y_1)\right]. \tag{A.21}$$

On solving (A.18) and (A.21), we get:

$$\psi(X_1, Y_1) = \frac{c_4}{4 - 3c_3c_4}\psi(X_2, Y_1), \tag{A.22}$$

where c_4 is defined as

$$c_4 = \left(1 + \sqrt{\frac{3}{8}}g\Delta X\right)^{-1} \tag{A.23}$$

and

$$\psi(X_1, Y_0) = \frac{c_3c_4}{4 - 3c_3c_4}\psi(X_2, Y_1). \tag{A.24}$$

Furthermore, it should be believed that ψ vanishes at the points far away from the origin (marked in blue) due to normalization condition, so if X_n or Y_n is large enough, ψ can be approximately be zero. Using this condition with (A.1), (A.8), (A.13), (A.15), (A.16), (A.22) and (A.24), the values of $\psi(X_i, Y_j)$ and $E_{X,Y}$ can be obtained numerically by diagonalization.

Appendix B

Solution for background with two non-interacting atoms

In Chapter 4, it was demonstrated that the spatial distribution for the impurity is directly related to the configuration of the system. If the background atoms are non-interacting, the energy and the wave function for the system will also be affected. For demonstration, we consider a system made up of two background atoms, which do not interact among themselves. However, the atoms interact with the impurity very strongly ($g \to \infty$). When the impurity is placed at the middle of the system, it sets an impenetrable barrier to the two background atoms. In this case, the system reduces to the case in Chapter 4. However, the energy of the system should be lowered if the impurity is placed at one side of the system. In this appendix, we provide an analytic solution to verify our ideas.

B.1 Time-independent Schrödinger's equation

Using the rescaled units in Chapter 3, the time-independent Schrödinger's equation for the system is

$$\begin{aligned}&\left[-\frac{1}{2}\left(\frac{\partial^2}{\partial x_1^2}+\frac{\partial^2}{\partial x_2^2}+\frac{\partial^2}{\partial y^2}\right)+\frac{x_1^2+x_2^2+y^2}{2}\right]\Psi\left(x_1,x_2;y\right)\\ =&E\Psi\left(x_1,x_2;y\right),\end{aligned} \tag{B.1}$$

with the boundary conditions $\Psi\left(x_1,x_2;y\right)=0$ when $x_1=y$ and $x_2=y$. Guided by the studies on three-atom system in Chapter 3, the same coordinate system in (3.16) is used:

$$\begin{pmatrix}X\\Y\\Z\end{pmatrix}=\begin{pmatrix}\frac{1}{\sqrt{3}} & \frac{1}{\sqrt{3}} & \frac{1}{\sqrt{3}}\\ -\frac{1}{\sqrt{2}} & \frac{1}{\sqrt{2}} & 0\\ -\frac{1}{\sqrt{6}} & -\frac{1}{\sqrt{6}} & \sqrt{\frac{2}{3}}\end{pmatrix}\begin{pmatrix}x_1\\x_2\\y\end{pmatrix}. \tag{B.2}$$

In the new coordinate system, the Hamiltonian can be separated into two different parts $H=H_{\mathrm{CM}}+H_{\mathrm{rel}}$ which are defined as

$$\begin{aligned}H_{\mathrm{CM}}&=-\frac{1}{2}\frac{\partial^2}{\partial X^2}+\frac{X^2}{2}\\ H_{\mathrm{rel}}&=-\frac{1}{2}\left(\frac{\partial^2}{\partial Y^2}+\frac{\partial^2}{\partial Z^2}\right)+\frac{Y^2+Z^2}{2}.\end{aligned} \tag{B.3}$$

Therefore, the wave function is factorized as $\Psi\left(X,Y,Z\right)=\phi\left(X\right)\psi\left(Y,Z\right)$ with the boundary condition given by $\psi\left(Y,Z\right)=0$ when $\left(Y+\sqrt{3}Z\right)/2=0$ and $\left(Y-\sqrt{3}Z\right)/2=0$.

Focusing on the equation $H_{\mathrm{rel}}\psi\left(Y,Z\right)=E_r\psi\left(Y,Z\right)$, we will solve it in polar co-ordinates. Defining $r=\sqrt{Y^2+Z^2}$ and $\theta=\tan^{-1}\left(Z/Y\right)$, the corresponding equation in polar co-ordinates is given by

$$\left[-\frac{1}{2}\left(\frac{\partial^2}{\partial r^2}+\frac{1}{r}\frac{\partial}{\partial r}+\frac{1}{r^2}\frac{\partial^2}{\partial\theta^2}\right)+\frac{r^2}{2}\right]\psi\left(r,\theta\right)=E_r\psi\left(r,\theta\right). \tag{B.4}$$

Clearly, (B.4) is equivalent to the equation for the two-dimensional isotropic harmonic potential. The solutions can be found in standard textbook [70].

However, the wave function $\psi(r,\theta)$ for the present system must satisfy the boundary conditions:

$$\psi(r,\pm\pi/6)=0 \quad \text{and} \quad \psi(r,\pm 5\pi/6)=0. \tag{B.5}$$

To take care of the configuration of the system, we notice that there is a one-to-one mapping between it and the region on the $Y-Z$ plane. The region and the mapping is shown in Fig. B.1 and Table B.1 respectively. Particularly, the reflection along the Z-axis represent the exchange in x_1 and x_2, so we require $\Theta(\theta)=\Theta(\pi-\theta)$ for proper symmetrization of the wave function.

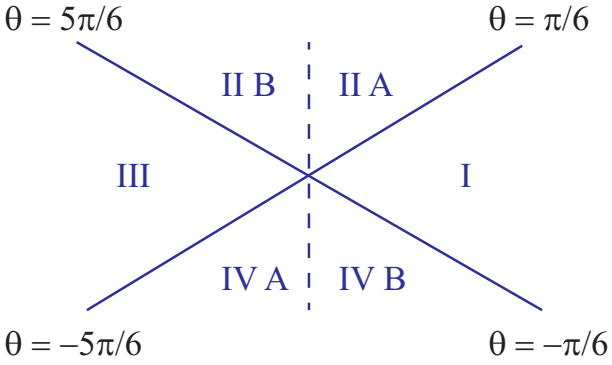

Figure B.1: Different regions for the angular equation.

B.2 Analytic solution

By separation of variables $\psi(r,\theta)=R(r)\,\Theta(\theta)$, the radial equation is

$$\left[\frac{d^2}{dr^2}+\frac{1}{r}\frac{d}{dr}+\left(2E_r-r^2-\frac{m^2}{r^2}\right)\right]R(r)=0. \tag{B.6}$$

The angular equation is

$$\frac{d^2}{d\theta^2}\Theta(\theta)=-m^2\Theta(\theta). \tag{B.7}$$

To solve (B.6), we write

$$R(r)=r^{|m|}e^{-r^2/2}G(r), \tag{B.8}$$

Region	Configuration
I	$x_1 < y < x_2$
II A	$x_1 < x_2 < y$
II B	$x_2 < x_1 < y$
III	$x_2 < y < x_1$
IV A	$y < x_2 < x_1$
IV B	$y < x_1 < x_2$

Table B.1: Mapping between the regions and the configurations of the system

which takes care of the asymptotic behaviour of $R(r)$ when $r \to 0$ and $r \to \infty$. Then, the radial equation becomes

$$\frac{d^2G(r)}{dr^2} + \left(\frac{2|m|+1}{r} - 2r\right)\frac{dG(r)}{dr} + 2(E_r - 1 - |m|)G(r) = 0. \quad \text{(B.9)}$$

The solution is given by

$$G(r) = L_{n_r}^{|m|}\left(r^2\right), \quad \text{(B.10)}$$

where $L_{n_r}^{|m|}(r^2)$ is the associated Laguerre polynomial [46]. Hence, we obtain the solution for $R(r)$:

$$R(r) = r^{|m|}e^{-r^2/2}L_{n_r}^{|m|}\left(r^2\right), \quad \text{(B.11)}$$

with the corresponding energy:

$$E_r = |m| + 2n_r + 1. \quad \text{(B.12)}$$

For the angular equation, it is clear that the general solution is

$$\Theta(\theta) = C_1\sin(m\theta) + C_2\cos(m\theta), \quad \text{(B.13)}$$

where C_1 and C_2 are arbitrary constants. However, the actual solution depends on the configuration of the system. Also, the solution must obey the boundary conditions. In the following, we will consider two different configurations separately.

B.2.1 Case 1: Impurity at the middle

First, we consider the case when the impurity is placed at the middle ($x_1 < y < x_2$). The corresponding region on the $Y - Z$ plane is $-\pi/6 < \theta < \pi/6$. Due to the boundary conditions $\Theta(-\pi/6) = \Theta(\pi/6) = 0$, the solution corresponds to the lowest energy is given by

$$\Theta(\theta) = \sin\left[3\left(\theta - \frac{\pi}{6}\right)\right], \tag{B.14}$$

with the pre-factor absorbed in the radial part of the solution. From (B.12), the ground state energy for the system is

$$E = 0.5 + 3 + 2(0) + 1 = 4.5, \tag{B.15}$$

which is the same as the ground state energy for the system with background of Tonks gas.

To understand the situation better, we write out the solution explicitly:

$$\Psi(X, r, \theta) = \mathcal{N}_1 e^{-\frac{X^2}{2}} e^{-\frac{r^2}{2}} r^3 L_0^3\left(r^2\right) \sin\left[3\left(\theta - \frac{\pi}{6}\right)\right], \tag{B.16}$$

with $\mathcal{N}_1$ being the normalization factor. It is noticed that $L_0^3(r^2) = 1$, so the solution in terms of x_1, x_2 and y is given by

$$\Psi(x_1, x_2, y) = \mathcal{N}_1 e^{-\frac{x_1^2 + x_2^2 + y^2}{2}} (x_2 - x_1)(y - x_1)(y - x_2). \tag{B.17}$$

This is precisely the solution for the system with background of Tonks gas.

B.2.2 Case 2: Impurity at the right-hand side

If the impurity is placed at the right-hand side ($x_1 < x_2 < y$), the corresponding region on the $Y - Z$ plane is $\pi/6 < \theta < 5\pi/6$. For this case, the solution corresponds to the lowest energy is modified as

$$\Theta(\theta) = \sin\left[\frac{3}{2}\left(\theta - \frac{\pi}{6}\right)\right]. \tag{B.18}$$

Therefore, the ground state energy changes to

$$E = 0.5 + 3/2 + 2\,(0) + 1 = 3, \tag{B.19}$$

which is lower than the previous case. Since the solution in terms of x_1, x_2 and y is very troublesome for this case, we do not display it here. Finally, it is reminded that the solutions for the remaining four configurations can be obtained easily by symmetry argument.

Appendix C

Derivation of the Fröhlich polaron Hamiltonian

In Chapter 5, we have used the Fröhlich polaron Hamiltonian to describe the interaction between the impurity atom and the Bogoliubov excitations of the condensate. Since the derivation of the Hamiltonian is non-trivial and difficult to be found in literature, it is desired for us to provide the derivation in this appendix.

It is reminded that the second quantized Hamiltonian for the system is given in (5.1):

$$\begin{aligned}\hat{H} = &\int \hat{\psi}^{\dagger}(x)\left[-\frac{\hbar^2}{2m_B}\frac{d^2}{dx^2}+\frac{g_{BB}}{2}\hat{\psi}^{\dagger}(x)\hat{\psi}(x)\right]\hat{\psi}(x)\,\mathrm{d}x \\ &+\int \hat{\phi}^{\dagger}(x)\left(-\frac{\hbar^2}{2m_I}\frac{d^2}{dx^2}\right)\hat{\phi}(x)\,\mathrm{d}x \\ &+g_{BI}\int \hat{\psi}^{\dagger}(x)\hat{\psi}(x)\hat{\phi}^{\dagger}(x)\hat{\phi}(x)\,\mathrm{d}x. \end{aligned} \tag{C.1}$$

Here, $\hat{\psi}(x)$ and $\hat{\phi}(x)$ stand for the field operators, which annihilate a condensate atom and the impurity atom at x respectively. Since both of the impurity atom and the condensate are untrapped, we expand the field operators by the

plane wave basis:

$$\hat{\psi}(x) = \sum_k \hat{a}_k \frac{e^{ikx}}{\sqrt{l}}, \quad \hat{\phi}(x) = \sum_k \hat{b}_k \frac{e^{ikx}}{\sqrt{l}}. \tag{C.2}$$

Here, $\hat{a}_k$ and $\hat{b}_k$ are the annihilation operators which annihilate a condensate atom and an impurity atom with wave number k. The Hamiltonian becomes

$$\begin{aligned}\hat{H} =& \sum_k \frac{\hbar^2 k^2}{2m_B} \hat{a}_k^\dagger \hat{a}_k + \frac{g_{BB}}{2l} \sum_{k_1,k_2,q} \hat{a}_{k_1+q}^\dagger \hat{a}_{k_2-q}^\dagger \hat{a}_{k_1} \hat{a}_{k_2} \\ &+ \sum_k \frac{\hbar^2 k^2}{2m_I} \hat{b}_k^\dagger \hat{b}_k + \frac{g_{BI}}{l} \sum_{k_1,k_2,q} \hat{a}_{k_2+q}^\dagger \hat{a}_{k_2} \hat{b}_{k_1-q}^\dagger \hat{b}_{k_1}.\end{aligned} \tag{C.3}$$

Since there is only one impurity atom, we have

$$\sum_k \frac{\hbar^2 k^2}{2m_I} \hat{b}_k^\dagger \hat{b}_k = \frac{\hat{p}^2}{2m_I}, \tag{C.4}$$

with $\hat{p}$ being the momentum operator for the impurity atom. Also, the last term in (C.3) can be written as

$$\frac{g_{BI}}{l} \sum_{k_1,k_2,q} \hat{a}_{k_2+q}^\dagger \hat{a}_{k_2} \hat{b}_{k_1-q}^\dagger \hat{b}_{k_1} = \frac{g_{BI}}{l} \sum_{k_1,k_2,q} \hat{a}_{k_2+q}^\dagger \hat{a}_{k_2} \left|k_1 - q\right\rangle \left\langle k_1\right|. \tag{C.5}$$

Switching to the position space representation for the impurity atom, we have

$$\begin{aligned}&\frac{g_{BI}}{l} \sum_{k_1,k_2,q} \hat{a}_{k_2+q}^\dagger \hat{a}_{k_2} \left|k_1 - q\right\rangle \left\langle k_1\right| \\ =&\frac{g_{BI}}{l} \sum_{k_1,k_2,q} \hat{a}_{k_2+q}^\dagger \hat{a}_{k_2} \int \mathrm{d}y \left|y\right\rangle \left\langle y\right| k_1 - q\rangle \int \mathrm{d}y' \left\langle k_1\right| y'\rangle \left\langle y'\right| \\ =&\frac{g_{BI}}{l} \sum_{k_1,k_2,q} \hat{a}_{k_2+q}^\dagger \hat{a}_{k_2} \int \mathrm{d}y \left|y\right\rangle \frac{e^{-i(k_1-q)y}}{\sqrt{l}} \int \mathrm{d}y' \frac{e^{ik_1 y'}}{\sqrt{l}} \left\langle y'\right| \\ =&\frac{g_{BI}}{l} \sum_{k_2,q} \hat{a}_{k_2+q}^\dagger \hat{a}_{k_2} \int\int \mathrm{d}y\mathrm{d}y' \left|y\right\rangle \left\langle y'\right| e^{iqy} \sum_{k_1} \frac{e^{ik_1(y'-y)}}{l} \\ =&\frac{g_{BI}}{l} \sum_{k_2,q} \hat{a}_{k_2+q}^\dagger \hat{a}_{k_2} \int \mathrm{d}y e^{iqy} \left|y\right\rangle \left\langle y\right| \\ =&\frac{g_{BI}}{l} \sum_{k,q} \hat{a}_k^\dagger \hat{a}_q e^{-i(k-q)\hat{y}}.\end{aligned} \tag{C.6}$$

Using the results in (C.4) and (C.6), the Hamiltonian becomes

$$\begin{aligned}\hat{H} =& \sum_{k} \frac{\hbar^2 k^2}{2m_B} \hat{a}_k^\dagger \hat{a}_k + \frac{g_{BB}}{2l} \sum_{k_1,k_2,q} \hat{a}_{k_1+q}^\dagger \hat{a}_{k_2-q}^\dagger \hat{a}_{k_1} \hat{a}_{k_2} \\ &+ \frac{\hat{p}^2}{2m_I} + \frac{g_{BI}}{l} \sum_{k,q} \hat{a}_k^\dagger \hat{a}_q e^{-i(k-q)\hat{y}}. \end{aligned} \tag{C.7}$$

Applying the Bogoliubov approximation discussed in 2.4.3, the Hamiltonian becomes

$$\begin{aligned}\hat{H} =& \frac{g_{BB} N^2}{2l} + \frac{g_{BI} N}{l} \\ &+ \frac{\hat{p}^2}{2m_I} + \sum_{k} \frac{\hbar^2 k^2}{2m_B} \hat{a}_k^\dagger \hat{a}_k + \frac{g_{BB} N}{2l} \sum_{k\neq 0} \left(\hat{a}_k^\dagger \hat{a}_{-k}^\dagger + 2\hat{a}_k^\dagger \hat{a}_k + \hat{a}_k \hat{a}_{-k} \right) \\ &+ \frac{g_{BI}\sqrt{N}}{l} \sum_{k\neq 0} \left(\hat{a}_k^\dagger e^{-ik\hat{y}} + \hat{a}_k e^{ik\hat{y}} \right) + \frac{g_{BI}}{l} \sum_{k\neq 0} \sum_{q\neq 0} \hat{a}_k^\dagger \hat{a}_q e^{-i(k-q)\hat{y}}. \end{aligned} \tag{C.8}$$

Since $\sqrt{N} \gg 1$, the last term for the Hamiltonian can be dropped. To diagonalize the Hamiltonian, we apply the Bogoliubov transformation in (2.47). Finally, we obtain $\hat{H} = E_0 + \hat{H}_{\text{pol}}$ which are given by

$$E_0 = \frac{g_{BB} N^2}{2l} + \frac{g_{BI} N}{l} + \sum_{k\neq 0} \frac{\xi(k) - g_{BB}\rho - \epsilon(k)}{2} \tag{C.9}$$

and

$$\hat{H}_{\text{pol}} = \frac{\hat{p}^2}{2m_I} + \sum_{k\neq 0} \xi(k) \hat{c}_k^\dagger \hat{c}_k + \sum_{k\neq 0} \frac{g_{BI}\sqrt{N}}{l} \frac{\epsilon(k)}{\xi(k)} \left(e^{ik\hat{y}} \hat{c}_k + e^{-ik\hat{y}} \hat{c}_k^\dagger \right). \tag{C.10}$$

Therefore, the derivation of the Fröhlich polaron Hamiltonian is completed.

Appendix D

Validity of the product form solution

In Chapter 5, the wave function for the impurity-condensate system was assumed to be factorized. In this appendix, we apply the first order perturbation theory on the Fröhlich polaron Hamiltonian to obtain the possible correction to the product form wave function. Using the rescaled units in (5.16), the correction depends on ζ solely when the mass ratio of the system is fixed.

To check the validity of the product form solution, we consider the possible correction due to quantum fluctuation. We write $\hat{c}_k = Z_k + \delta\hat{c}_k$, with Z_k defined in (5.26). Then, the Hamiltonian becomes $\hat{H}_{\text{pol}} = \hat{H}_0 + \hat{H}_1$, where $\hat{H}_0$ and $\hat{H}_1$ are defined as

$$\hat{H}_0 = \frac{\hat{p}^2}{2m_I} + \sum_{k\neq 0} 2Z_k V_k \cos ky + \sum_{k\neq 0} \xi(k) Z_k^2 \tag{D.1}$$

and

$$\begin{aligned}\hat{H}_1 = &\sum_{k\neq 0} \xi(k)\, \delta\hat{c}_k^\dagger \delta\hat{c}_k + \sum_{k\neq 0} \xi(k) Z_k \left(\delta\hat{c}_k + \delta\hat{c}_k^\dagger\right) \\ &+ \sum_{k\neq 0} V_k \cos ky \left(\delta\hat{c}_k + \delta\hat{c}_k^\dagger\right) + i\sum_{k\neq 0} V_k \sin ky \left(\delta\hat{c}_k - \delta\hat{c}_k^\dagger\right).\end{aligned} \tag{D.2}$$

Here, $\hat{H}_0$ stands for the Hamiltonian corresponds to the previous studies. The second term for $\hat{H}_0$ is the effective trapping potential due to the interaction between the impurity atom and the Bogoliubov excitations. Due to this potential, the impurity atom can self-localize in a homogeneous condensate.

For $\hat{H}_1$, we treat it as perturbation. We denote the product state as $\left|\Psi^{(0)}\right\rangle = |0\rangle \otimes \left|\tilde{0}\right\rangle$. Here, the impurity atom is in the ground state of the effective trapping potential and $\left|\tilde{0}\right\rangle$ stands for the displaced Bogoliubov vacuum for the condensate, defined as

$$\delta\hat{c}_k \left|\tilde{0}\right\rangle = 0 \tag{D.3}$$

The correction to $\left|\Psi^{(0)}\right\rangle$ contributed mostly from the state $|1\rangle \otimes \left|\tilde{1}_k\right\rangle$ due to the fluctuation. Here, $\left|\tilde{1}_k\right\rangle$ is defined as

$$\delta\hat{c}_k^\dagger \left|\tilde{0}\right\rangle = \left|\tilde{1}_k\right\rangle \tag{D.4}$$

Hence, we write the perturbed state as

$$|\Psi'\rangle = \frac{1}{\sqrt{1+\sum_k |B_k|^2}} \left[|0\rangle \otimes \left|\tilde{0}\right\rangle + \sum_{k\neq 0} B_k |1\rangle \otimes \left|\tilde{1}_k\right\rangle \right]. \tag{D.5}$$

According to first order perturbation theory, B_k are given by

$$B_k = \frac{\langle 1| \otimes \langle\tilde{1}_k| \hat{H}_1 |0\rangle \otimes \left|\tilde{0}\right\rangle}{E_0 - E_1}, \tag{D.6}$$

where E_0 and E_1 stand for the energies for the states $|0\rangle \otimes \left|\tilde{0}\right\rangle$ and $|1\rangle \otimes \left|\tilde{1}_k\right\rangle$ respectively. We plot $\sum_k |B_k|^2 / \left(1+\sum_k |B_k|^2\right)$ against ζ for $\alpha = 7/85$ and $\alpha = 23/85$ in Fig. D.1. From the figure, we see that the corrections are less than 3% to 5%, which shows that the product form solution is a good approximation to the ground state wave function of the system.

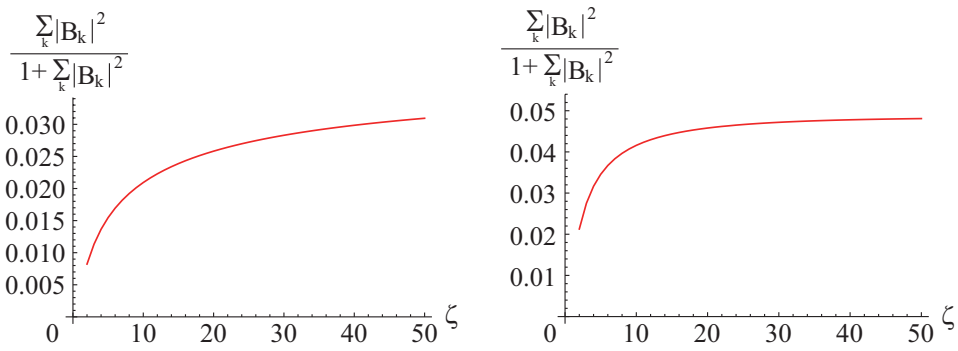

Figure D.1: The correction to the product form solution when $\alpha = 7/85$ (left) and $\alpha = 23/85$ (right).